Japanese Journal of Gastroenterology and Hepatology

Research Article

ISSN: 2435-1210 | Volume 9

Identification of Polyamine Subtypes in Hepatocellular Carcinoma and Characteristics of their Immune Infiltrates

Xu Y[1], Hao X[2], Xu QC[2], Ren Y[2], Liu X[2], Wang Y[2], Song S[1*] and Wang Q[3*]

[1]Marine College, Shandong University, China

[2]Department of Clinical Laboratory, The Second Hospital of Shandong University, China

[3]Department of Anesthesiology, Qilu Hospital, Cheeloo College of Medicine, Shandong University, China

***Corresponding author:**

Shuliang Song,
Marine College, Shandong University, Weihai 264209, China, Tel: +8613721935592;
E-mail: songshuliang@sdu.edu.cn

Qin Wang,
Department of Anesthesiology, Qilu Hospital, Cheeloo College of Medicine, Shandong University, 107 Wenhua Xi Road, Jinan 250012, China,
Tel: +8618560088139;
E-mail: wangqin8207@163.com

Received: 08 Jul 2022
Accepted: 18 Jul 2022
Published: 23 Jul 2022
J Short Name: JJGH

Keywords:

Hepatocellular carcinoma; Polyamine metabolism-related genes; Tumor microenvironment; Immunotherapy; Sorafenib resistance

Citation:

Song S, Wang Q. Identification of Polyamine Subtypes in Hepatocellular Carcinoma and Characteristics of their Immune Infiltrates. J Gstro Hepato. V9(3): 1-22

1. Abstract

1.1. Background: Hepatocellular Carcinoma (HCC) is one of the leading causes of cancer-related death. Due to the poor prognosis of standard treatment, it is urgent to evaluate the immune molecular characteristics and find new HCC immune biomarkers and immunotherapy . The homeostasis of polyamines is closely related to tumor progression and prognosis. The uptake of polyamines by immune cells also leads to a decrease in anti-tumor cytokines and the anti-tumor ability of immune cells. Therefore, having a thorough understanding of the features of tumor microenvironment cell invasion driven by complex polyamine metabolism-related genes (PMRGs) may be helpful for identifying the potential mechanisms of HCC occurrence and forecasting the effectiveness of immunotherapy.

1.2. Methods: In this study, we analyzed the genetic alterations and expression patterns of PMRGs. We then constructed PMRG_Score to predict relapse-free survival .

1.3. Results: We obtained three different polyamine subtypes, and found that the different expression patterns of PMRGs were closely related to the tumor microenvironment and prognosis of HCC. The high expression of PMRGs causes a more complex immune microenvironment and poor prognosis. High PMRG_Score was accompanied by increased expression levels of immune checkpoints and an immunosuppressive microenvironment.

1.4. Conclusions: The PMRGs may play an immunosuppressive role in HCC, and patients with high PMRGs expression are more likely to benefit from immune checkpoint inhibitors. The research is a great help to evaluating the prognosis of liver cancer and the subsequent development of more effective immunotherapy strategies.

2. Highlight

- It is urgent to evaluate the immune molecular characteristics and provide more information for finding new HCC immune biomarkers and immunotherapy during the tumor evolution of HCC
- The different expression patterns of PMRGs were closely related to the tumor microenvironment and prognosis of HCC.
- The PMRGs play an immunosuppressive role in HCC, and patients with high PMRGs expression are more likely to benefit from immune checkpoint inhibitors.

3. Introduction

Hepatocellular Carcinoma (HCC), the sixth leading cancer type, is the third leading cause of cancer-related death worldwide [1], and currently the most common primary liver cancer, accounting for 90% of all primary liver cancers [2]. Chronic HBV infection and chronic HCV infection are the leading causative causes of hepatocellular carcinoma, and hepatitis virus and Nonalcoholic Fatty Liver Disease (NAFLD) increase the risk of hepatocellular carcinoma [3, 4]. The multi-targeted Tyrosine Kinase Inhibitor (TKI) sorafenib is the only first-line drug approved by the U.S. Food and Drug Administration (FDA) to treat advanced HCC [5, 6]. However, patient prognosis remains poor, as the response rate to sorafenib is less than 5%, even 70% of patients can't benefit from sorafenib, the median overall survival has not been effectively prolonged [7], which is a large part of the reason comes from sorafenib resistance.

The tumor microenvironment predominantly affects the occurrence, metastasis, invasion, and sorafenib resistance of HCC, which contains complex interactions between various immune and non-immune cells. Immune cells such as Tumor-Associated Macrophages (TAMs) [8], Tumor-Associated Neutrophils (TAN) [9], regulatory T cells (Tregs) [10] and M2 macrophages [11] maintain tumor growth and metastasis by secreting a variety of cytokines. Immunotherapy is a promising therapeutic tool for many cancers, especially virus-induced cancers, so immunotherapy is a promising treatment for HCC [12]. Programmed cell death protein 1 (PD-1) inhibitors and cytotoxic T lymphocyte-associated protein 4 (CTLA4) inhibitors have shown significant benefits in treating various tumors, such as melanoma, non-small cell carcinoma, and renal cell carcinoma [13-17].

Polyamines mainly include putrescine, spermine, and spermidine, a class of positively charged alkylamine small molecules ubiquitous in living organisms [18]. Their homeostasis is critical for maintaining normal cell growth and proliferation. In contrast, polyamine metabolism is dysregulated in multiple tumor states. In various cancers, polyamine levels are elevated, and crosstalk occurs between polyamine metabolism and multiple oncogenic pathways such as WNT signaling, mTORC1, and the RAS pathway [19-23]. The uptake of polyamines by immune cells reduces the mRNA expression of adhesion molecules involved in anti-tumor immunity, such as CD56 and CD11a, and decreases cytokine production required for anti-tumor activity and anti-tumor immune function of immune cells [24]. Recent studies have shown that polyamine-mediated autophagy inhibits M1 polarization of macrophages, while up-regulation of ATG5 expression promotes M2 polarization of Kupffer cells. Pretreatment of Kupffer cells with spermine decreased CCL2, CXCL-10, TNF-α, and IL-6 but increased IL-10 in the tissue, thereby inhibiting the recruitment of immune cells [25]. Polyamine metabolism acts on autoimmune inflammation and anti-tumor immunity, polyamine depletion increases inflammation, and polyamine enrichment enhances immunosuppression of myeloid cells [26]. The rapid proliferation of cancer cells and the anti-tumor immune function of immune cells depend on high intracellular polyamine levels, and high polyamine content in tumor tissue is also an important indicator of poor prognosis in cancer patients. Thus polyamines may serve as general therapeutic targets for cancer therapy and monitor immune responses and tumor cell reactions to immunotherapy [27].

Multiple genes interact in a highly coordinated way to produce anti-tumor effects. The role of Polyamine Metabolism-Related Genes (PMRGs) in the HCC microenvironment remains not clear. Therefore, having a thorough understanding of the features of tumor microenvironment cell invasion driven by complex Polyamine Metabolism-Related Genes (PMRGs) may be helpful for identifying the potential mechanisms of HCC occurrence and forecasting the effectiveness of immunotherapy. This research analyzes the transcriptional patterns of PMRGs in primary hepatocellular carcinoma and compares the enrichment of functional pathways and immune patterns between different subtypes through multiple algorithms. The comprehensive analysis revealed the effect of PMRGs on the immune microenvironment of HCC and its crucial clinical significance and provided a new idea for guiding personalized immunotherapy strategies for HCC patients.

4. Methods

4.1. Data sources

We downloaded gene expression (FPKM) and associated prognostic and clinical data from 160 healthy liver tissue samples and 371 liver cancer tissue samples from The Cancer Genome Atlas (TCGA) database and the Genotype-Tissue Expression (GTEx) database(https://xenabrowser.net/datapages/).

4.2. Consensus clustering analysis

We obtained 35 PMRGs from published articles. All specific information about the genes mentioned above can be found in Supplementary Table 1. We classified patients into different molecular subtypes based on the mRNA level of PMRGs by Package "ConensusClusterPlus". Different polyamine-related subtypes associated with PMRGs expression were identified by the k-means method. The number of clusters and their stability were determined by Cumulative Distribution Function (CDF) curves, intra-group correlations, and inter-group correlations. We performed 1000 repetitions to guarantee the stability of the classification.

Supplementary Table 1: The polyamine metabolism-related genes.

Gene	Type
ODC1	polyamine metabolism
SRM	polyamine metabolism
SMS	polyamine metabolism
AMD1	polyamine metabolism
CEP131	polyamine metabolism
DHPS	polyamine metabolism
EIF5A	polyamine metabolism
MAT2A	polyamine metabolism
PAOX	polyamine metabolism
SAT2	polyamine metabolism
SAT1	polyamine metabolism
SMOX	polyamine metabolism
SLC22A16	polyamine metabolism
SLC3A2	polyamine metabolism
ARG1	polyamine metabolism
ARG2	polyamine metabolism
CPS1	polyamine metabolism
OTC	polyamine metabolism
AZIN1	polyamine metabolism
AZIN2	polyamine metabolism
OAZ1	polyamine metabolism
OAZ2	polyamine metabolism
OAZ3	polyamine metabolism
SPR	polyamine metabolism
NNMT	polyamine metabolism
TP53	polyamine metabolism
MYC	polyamine metabolism
PPP6C	polyamine metabolism
IL17A	polyamine metabolism
AGMAT	polyamine metabolism
AOC1	polyamine metabolism
SOX2	polyamine metabolism
KLF4	polyamine metabolism
NANOG	polyamine metabolism
KDM1A	polyamine metabolism

4.3. Relationship between Polyamine subtypes with the clinical features and prognosis of HCC

We compared the relationship between polyamine subtypes, clinicopathological features, and prognosis to test the clinical value of the three subtypes identified by consensus clustering. We used Kaplan-Meier curves generated by the "survival" and "survminer" R packages to assess differences in Recurrence-Free Survival (RFS) between subtypes.

4.4. Calculation of TME Scores and PD-1/PD-L1 expression in HCC

We assessed each patient's immunity using the ESTIMATE algorithm. Additionally, the proportion of immune infiltration in each HCC patient was estimated using the CiberSort algorithm. TME scores for the three subtypes were assessed using the ESTIMATE package. The PD-1/PD-L1 levels are compared between the three clusters.

4.5. Differentially expressed genes (DEGs) certification and their enrichment analysis

We used "Limma" package to identify DEGs between different subtypes of PMRGs with a logFC of 1.5 and an adjusted p-value < 0.05. GO, and KEGG functional enrichment analyses were performed using R to figure out the possible functions of polyamine metabolism DEGs.

4.6. Gene Set Variation Analysis (GSVA) and Gene Set Enrichment Analysis (GSEA)

We performed GSVA enrichment analysis for polyamine subtypes with "GSVA" R package based on "c2.cp.kegg.v7.5.1.symbols" downloaded from the MSigDB database. The fold changes of genes in different subtypes were calculated and ranked using the "limma" package in R, and then GSEA analysis was performed . A p-value < 0.05 was considered statistically significant.

4.7. Statistical Analyses

All statistical analyses were performed using R version 4.0.3. Statistical significance was set at $p < .05$.

5. Results

5.1. Genetic and transcriptional alterations of polyamine metabolism-related genes in HCC

According to the gene set on the MSigDB platform and the existing literature, a total of 35 Polyamine Metabolism-Related Genes (PMRGs) (Supplementary Table 1) were included in this study, and their potential interaction networks were analyzed using the STRING database (Figure 1A). Next, we performed a pooled analysis of mutation rates in the 35 PMRGs. The result revealed a low mutation frequency in HCC. Among 364 HCC samples, 125 (34.34%) had PMRGs mutations, of which TP53 is the gene with the highest mutation rate (28%), and then CPS1, and nearly half of PMRGs had no mutation (SMS, AMD1, DHPS, MAT2A, PAOX, SAT1, SAT2,TP ARG2, OTC, OAZ1, OAZ2, OAZ3, NNMT, AGMAT, SOX2, KLF4) (Figure 1B). We then identified the mutation types of these PMRGs and their chromosomal location in HCC and found that TP53 had the most complex mutation type, with missense mutations being the most common mutation type (Figure 1C and Supplementary Table 2).

We also analyzed the differences in polyamine metabolism-related genes expression between normal and liver cancer tissues. The result showed that most genes involved in polyamine anabolism (such as ODC1, AGMAT, SMS) were up-regulated in tumor tissues compared to normal tissues, whereas most genes involved in polyamine breakdown and transport (such as SAT1, SAT2, SLC22A16, SLC3A2) were down-regulated in tumor tissues (Figure 1D, E). Our analysis showed that the genetic pattern and mRNA levels of PMRGs were significantly different in tumor and healthy samples, suggesting a potential function of PMRGs in HCC.

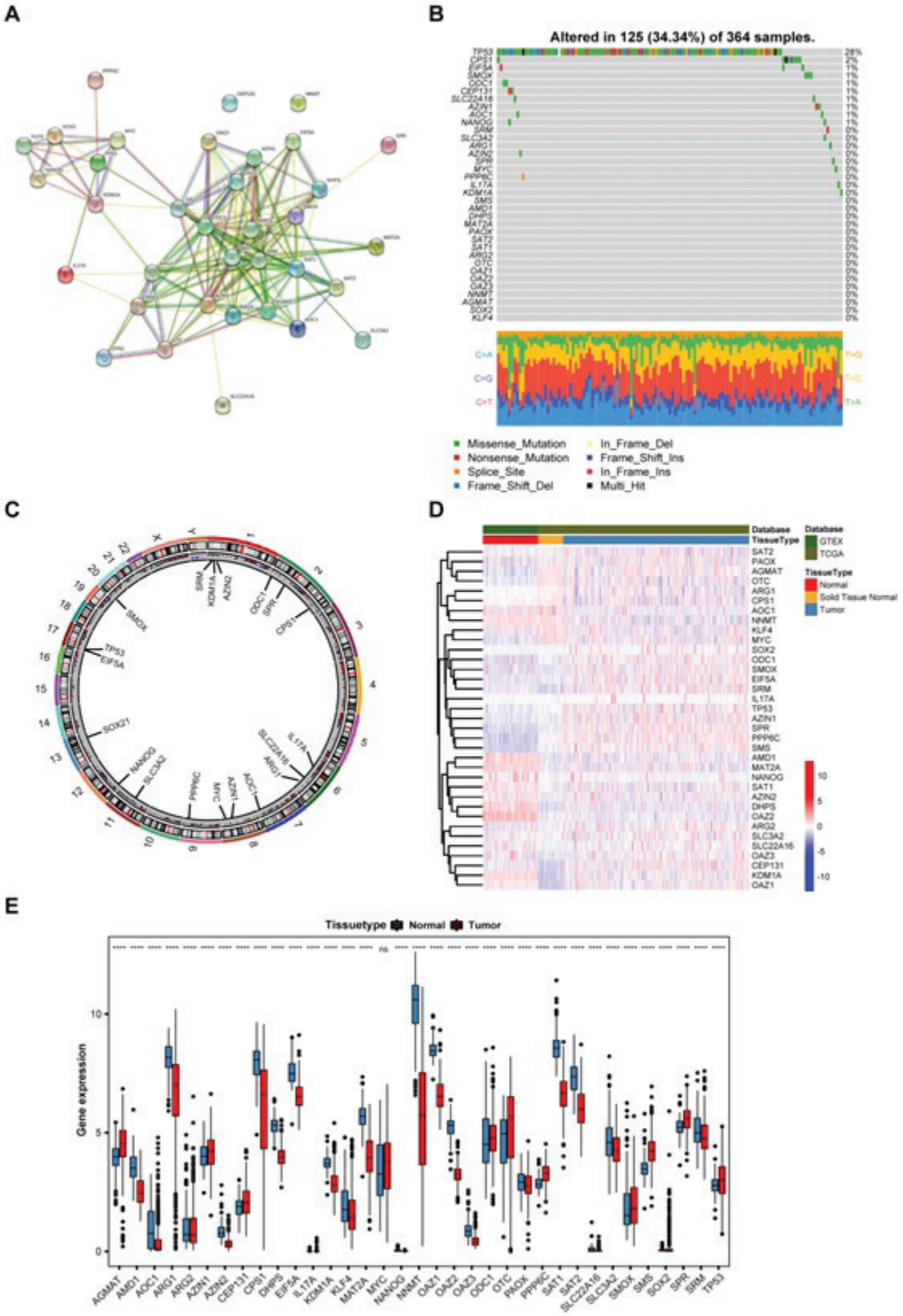

Figure 1: Genetic and transcriptional alterations of 35 PMRGs in HCC.

(A) PPI network showing the interactions of the PMRGs. (B) The oncoplot of mutation frequencies of 35 PMRGs in 364 HCC patients from TCGA. (C) The location of PMRGs on 23 chromosomes. (D) The heatmap of different mRNA levels of 35 PMRGs between normal liver tissue and tumor. (E) The expression distribution of 35 PMRGs between normal and HCC tissues. PMRGs, polyamine metabolism-related genes.

Supplementary Table 2: The mutation types of PMRGs and their chromosomal localization in HCC.

Hugo_Symbol	Chromosome	Start_Position	End_Position	Variant_Classification
TP53	chr17	7673764	7673764	Missense_Mutation
TP53	chr17	7673548	7673548	Frame_Shift_Del
TP53	chr17	7673550	7673579	In_Frame_Del
TP53	chr17	7674887	7674887	Missense_Mutation
TP53	chr17	7674252	7674252	Missense_Mutation
TP53	chr17	7674216	7674216	Missense_Mutation
TP53	chr17	7674213	7674220	Frame_Shift_Del
TP53	chr17	7673705	7673715	Frame_Shift_Del
TP53	chr17	7675207	7675207	Nonsense_Mutation
TP53	chr17	7673610	7673610	Splice_Site
TP53	chr17	7673796	7673796	Missense_Mutation
TP53	chr17	7674227	7674227	Missense_Mutation
TP53	chr17	7674953	7674953	Missense_Mutation
TP53	chr17	7673704	7673704	Nonsense_Mutation
TP53	chr17	7674972	7674972	Splice_Site
TP53	chr17	7675092	7675092	Missense_Mutation
TP53	chr17	7675184	7675185	Frame_Shift_Ins
TP53	chr17	7674917	7674917	Missense_Mutation
TP53	chr17	7675236	7675236	Missense_Mutation
TP53	chr17	7675139	7675139	Missense_Mutation
TP53	chr17	7675160	7675160	Missense_Mutation
TP53	chr17	7673802	7673802	Missense_Mutation
TP53	chr17	7674872	7674872	Missense_Mutation
TP53	chr17	7673803	7673803	Missense_Mutation
TP53	chr17	7674859	7674859	Splice_Region
TP53	chr17	7673793	7673793	Missense_Mutation
TP53	chr17	7676273	7676273	Splice_Site
TP53	chr17	7674947	7674947	Missense_Mutation
TP53	chr17	7674292	7674292	Splice_Site
TP53	chr17	7674942	7674942	Missense_Mutation
TP53	chr17	7674917	7674917	Missense_Mutation
TP53	chr17	7674887	7674887	Missense_Mutation
TP53	chr17	7675182	7675182	Nonsense_Mutation
TP53	chr17	7675136	7675137	In_Frame_Ins
TP53	chr17	7674229	7674229	Missense_Mutation
TP53	chr17	7674216	7674216	Missense_Mutation
TP53	chr17	7674919	7674920	Frame_Shift_Del
TP53	chr17	7674953	7674953	Missense_Mutation
TP53	chr17	7674216	7674216	Missense_Mutation
TP53	chr17	7673610	7673610	Splice_Site
TP53	chr17	7674251	7674251	Missense_Mutation
TP53	chr17	7675145	7675145	Missense_Mutation
TP53	chr17	7673777	7673777	Missense_Mutation
TP53	chr17	7675994	7675994	Splice_Region
TP53	chr17	7673808	7673808	Missense_Mutation
TP53	chr17	7676203	7676203	Frame_Shift_Del
TP53	chr17	7675143	7675143	Missense_Mutation
TP53	chr17	7675206	7675206	Nonsense_Mutation
TP53	chr17	7674213	7674213	Frame_Shift_Del
TP53	chr17	7675237	7675237	Splice_Site
TP53	chr17	7673704	7673704	Nonsense_Mutation
TP53	chr17	7674870	7674870	Nonsense_Mutation
TP53	chr17	7673797	7673797	Missense_Mutation
TP53	chr17	7675236	7675236	Missense_Mutation
TP53	chr17	7675131	7675131	Missense_Mutation
TP53	chr17	7676031	7676031	Missense_Mutation
TP53	chr17	7674921	7674921	Nonsense_Mutation
TP53	chr17	7674216	7674216	Missense_Mutation
TP53	chr17	7675084	7675084	Missense_Mutation
TP53	chr17	7674957	7674957	Nonsense_Mutation
TP53	chr17	7674957	7674957	Nonsense_Mutation
TP53	chr17	7673824	7673824	Missense_Mutation
TP53	chr17	7674946	7674952	Frame_Shift_Del
TP53	chr17	7673789	7673789	Nonsense_Mutation
TP53	chr17	7673781	7673781	Missense_Mutation

TP53	chr17	7675159	7675186	Frame_Shift_Del
TP53	chr17	7673794	7673795	Frame_Shift_Ins
TP53	chr17	7674271	7674276	In_Frame_Del
TP53	chr17	7674220	7674220	Missense_Mutation
TP53	chr17	7674893	7674893	Missense_Mutation
TP53	chr17	7670715	7670715	Missense_Mutation
TP53	chr17	7674220	7674220	Missense_Mutation
TP53	chr17	7674216	7674216	Missense_Mutation
TP53	chr17	7673823	7673823	Missense_Mutation
TP53	chr17	7674221	7674221	Missense_Mutation
TP53	chr17	7674216	7674216	Missense_Mutation
TP53	chr17	7673545	7673545	Frame_Shift_Del
TP53	chr17	7674216	7674216	Missense_Mutation
TP53	chr17	7674193	7674193	Missense_Mutation
TP53	chr17	7673802	7673802	Missense_Mutation
TP53	chr17	7674220	7674220	Missense_Mutation
TP53	chr17	7674277	7674280	Frame_Shift_Del
TP53	chr17	7675237	7675237	Splice_Site
TP53	chr17	7673789	7673789	Nonsense_Mutation
TP53	chr17	7670717	7670717	Splice_Site
TP53	chr17	7675195	7675195	Missense_Mutation
TP53	chr17	7674893	7674893	Missense_Mutation
TP53	chr17	7676071	7676081	Frame_Shift_Del
TP53	chr17	7674216	7674216	Missense_Mutation
TP53	chr17	7673831	7673832	Frame_Shift_Ins
TP53	chr17	7674917	7674917	Missense_Mutation
TP53	chr17	7670688	7670688	Missense_Mutation
TP53	chr17	7676051	7676051	Missense_Mutation
TP53	chr17	7673832	7673832	Frame_Shift_Del
TP53	chr17	7676102	7676102	Frame_Shift_Del
TP53	chr17	7675143	7675143	Missense_Mutation
TP53	chr17	7674254	7674254	Frame_Shift_Del
TP53	chr17	7674206	7674206	Missense_Mutation
TP53	chr17	7674953	7674953	Missense_Mutation
TP53	chr17	7674216	7674216	Missense_Mutation
TP53	chr17	7673835	7673835	Frame_Shift_Del
CPS1	chr2	210577467	210577467	Nonsense_Mutation
CPS1	chr2	210663144	210663144	Missense_Mutation
CPS1	chr2	210660510	210660510	Missense_Mutation
CPS1	chr2	210594539	210594539	Missense_Mutation
CPS1	chr2	210647950	210647950	Missense_Mutation
CPS1	chr2	210606911	210606911	Missense_Mutation
CPS1	chr2	210590816	210590816	Missense_Mutation
CPS1	chr2	210608462	210608462	Missense_Mutation
CPS1	chr2	210591864	210591865	Frame_Shift_Ins
EIF5A	chr17	7309679	7309679	Nonsense_Mutation
EIF5A	chr17	7309656	7309656	Missense_Mutation
EIF5A	chr17	7309711	7309711	Missense_Mutation
SMOX	chr20	4182750	4182750	Missense_Mutation
SMOX	chr20	4175246	4175246	Missense_Mutation
SMOX	chr20	4182740	4182740	Missense_Mutation
ODC1	chr2	10441537	10441537	Missense_Mutation
ODC1	chr2	10440843	10440843	Missense_Mutation
CEP131	chr17	81219899	81219899	Missense_Mutation
CEP131	chr17	81194068	81194068	Nonsense_Mutation
IL17A	chr6	52189096	52189096	Missense_Mutation
SLC22A16	chr6	110442645	110442645	Missense_Mutation
SLC22A16	chr6	110431252	110431252	Missense_Mutation
AZIN2	chr1	33092210	33092210	Missense_Mutation
KDM1A	chr1	23083239	23083239	Missense_Mutation
AZIN1	chr8	102829914	102829914	Missense_Mutation
AZIN1	chr8	102843589	102843589	Nonsense_Mutation
AOC1	chr7	150857090	150857090	Missense_Mutation
AOC1	chr7	150858871	150858871	Missense_Mutation
NANOG	chr12	7793031	7793031	Missense_Mutation
NANOG	chr12	7794980	7794980	Missense_Mutation
PPP6C	chr9	125158384	125158384	Splice_Site
SRM	chr1	11059275	11059275	Nonsense_Mutation

SLC3A2	chr11	62881330	62881330	Missense_Mutation
MYC	chr8	127738755	127738755	Missense_Mutation
ARG1	chr6	131583834	131583834	Missense_Mutation
SPR	chr2	72887514	72887514	Missense_Mutation

5.2. Identification of polyamine metabolism subtypes in HCC

To comprehensively understand the expression characteristics and biological functions of PMRGs in tumorigenesis, we collected 371 patients from the liver cancer cohort (TCGA-LIHC) for further analysis. We grouped HCC patients multiple times on the basis of the mRNA levels of 35 PMRGs using the R Package "ConensusClusterPlus" (Supplementary Figure 1-3). The entire cohort was divided into cluster1 (n = 94), cluster2 (n = 120) and cluster3 (n = 157) with k=3 (Figure 2A). The expression levels and clinicopathological characteristics of PMRGs displayed dramatic differences between the three subtypes, with PMRGs having higher expression levels in cluster1 than in cluster2 and 3, and cluster1 preferentially associated with higher tumor grade and TNM Stage correlation (Figure 2B). Next, we performed a survival analysis of different subtypes based on the clustering results, and Kaplan-Meier curves showed that cluster1 patients had a shorter RFS than cluster 2,3 patients ($p<0.05$; Figure 2C). Finally, we performed principal component analysis, and PCA result further showed distinct PMRGs transcription profiling between these three subtypes (Figure 2D).

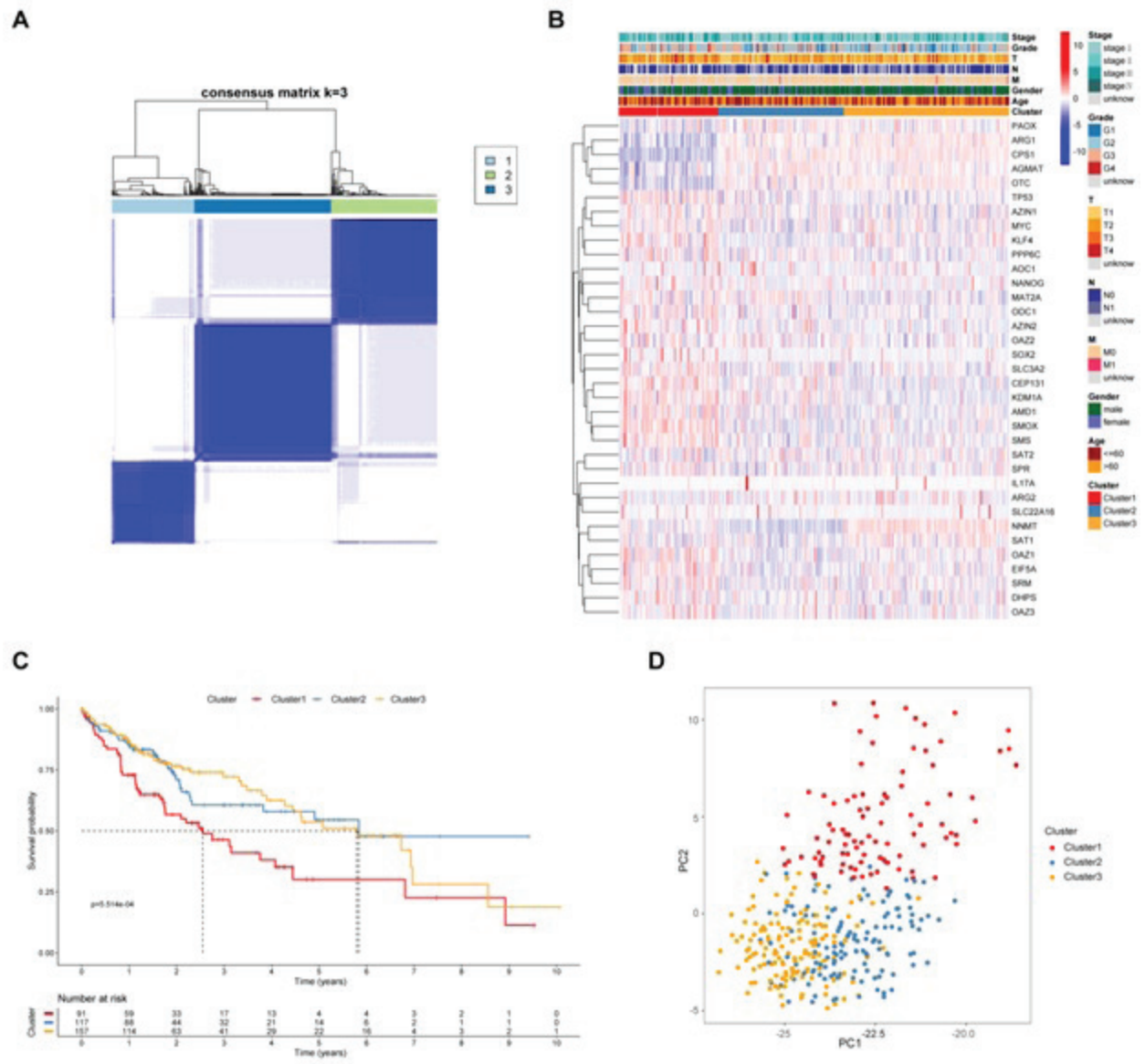

Figure 2: HCC classification and clinicopathological characteristics based on PMRGs by consensus clustering.
(A) Consensus matrix heatmap defining three clusters (k = 3) and their correlation area. (B) The heatmap of mRNA levels of 35 PMRGs in three polyamine subtypes. (C) Kaplan-Meier curves of OS based on polyamine subtypes in HCC patients. (D) PCA shows a remarkable difference in the expression of PMGRs. PMRGs, polyamine metabolism-related genes; OS, overall survival; PCA, principal component analysis.

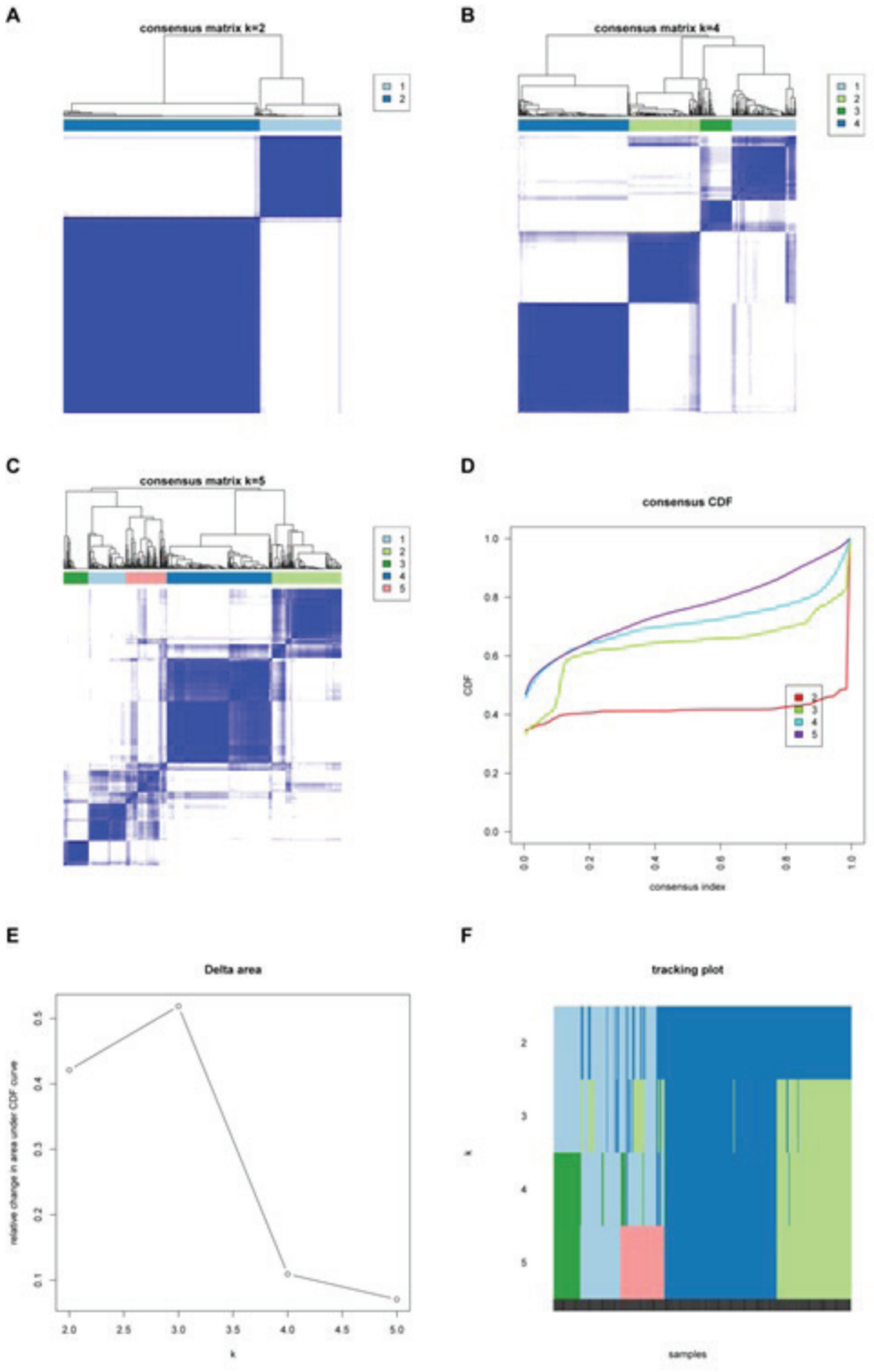

Supplementary Figure 1: Consensus clustering of pyroptosis-related genes in HCC.

(A-C) Consensus clustering of pyroptosis-related genes in TCGA-LIHC cohorts and consensus matrices for k = 2,4,5. (D-E) The consensus CDF curves and relative change in area under the CDF curve were shown for different k from 2 to 5. (F) The tracking plot provided a view of item cluster membership across different k in TCGA-LIHC cohorts.

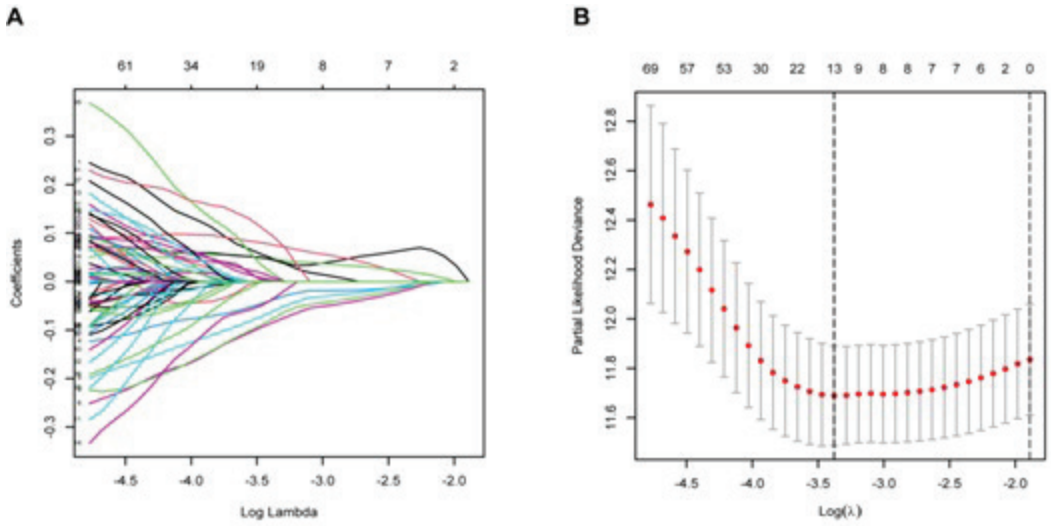

Supplementary Figure 2: Identifying representative candidate prognostic genes.
(A-B) The LASSO regression analysis and partial likelihood deviance on the prognostic genes.

5.3. Abundance analysis of immune cells infiltrating and characteristics of the TME in distinct subtypes

Given the role of polyamines in autoimmune inflammation and antitumor immunity, we analyzed the role of PMRGs in the TME. We assessed the abundance of 22 human immune cells in the tumor microenvironments of these three subtypes. We found that the immune infiltration is significantly different between cluster1 and cluster2 (Figure 3A). The infiltration levels of plasma cells, CD8+ T cells, CD4 memory-activated T cells, resting CD4 memory T cells, follicular helper T cells, regulatory T cells (Tregs), M0 macrophages, resting dendritic cells were higher in the cluster1 than those in the cluster 2. In contrast, the infiltration levels of naive B cells, M1 and M2 macrophages, and resting mast cells were remarkably lower in cluster1 than in cluster2. Next, we analyzed the two critical immune checkpoints, and observed that the mRNA levels of PD1/PD-L1 is higher in cluster1 (Figure 3B, C). ESTIMATE package was used to estimate the three subtype TME scores (ESTIMATEScore, ImmuneScores, and StomalScore). For TME scores, higher ImmuneScores and StomalScore represent the relatively high content of TME intermediate or immune cells, and ESTIMATEScore indicates the gathering of TME intermediate quality or immune scores. We found that the TME score in cluster1 had a higher TME score (Figure 3D), but patients in cluster2 had higher tumor purity (Figure 3E).

5.4. Functional enrichment analysis based on polyamine subtypes in HCC

To further understand the immunobiological differences between various polyamine subtypes, we performed the GSVA enrichment analysis. We observed that cluster1 was remarkably enriched in the immune activation pathway, such as NOD-like, Toll-like, and RIG-I-like receptor signaling pathways, natural killer cell-mediated cytotoxicity, T cell receptor signaling pathway, B cell receptor signaling pathway, antigen processing and presentation, cytokine receptor interaction, and chemokine signaling pathway activation (Figure 4A).

We further explored the underlying biological behavior of polyamine metabolic mechanism, and used the R package "LIMMA" to identify 244 differentially expressed genes (DEGs) associated with polyamine metabolic subtypes based on thresholds log2FC > 1.5 and $p < 0.05$. Fifty-six DEGs were enriched in cluster1, including some chemokines CXCL1, CXCL8, CCL20, and the innate immune checkpoint CD24 (Figure 4B, Supplementary Table 3). GO analysis showed that these genes associated with polyamine metabolic isoforms were significantly enriched in biological processes related to metabolism (Figure 4C). KEGG analysis indicated that biosynthetic metabolism and catabolism-related pathways were enhanced (Figure 4D). We also carried out the Gene Set Enrichment Analysis (GSEA) on 91 cluster1 and 120 cluster2 HCC samples. The results showed that cluster1 was significantly enriched among 233 biological processes, and we selected 6 biological processes related to immunity: REGULATION OF IMMUNE RESPONSE(NES=2.329, size=50), HUMORAL IMMUNE RESPONSE(NES=2.403, size=39), IMMUNE RESPONSE(NES=2.799, size=90), POSITIVE REGULATION OF IMMUNE SYSTEM PROCESS(NES=2.479, size=64), INNATE IMMUNE RESPONSE(NES=2.455, size=52, REGULATION OF LYMPHOCYTE ACTIVATION(NES=2.914, size=33) (Figure 5).

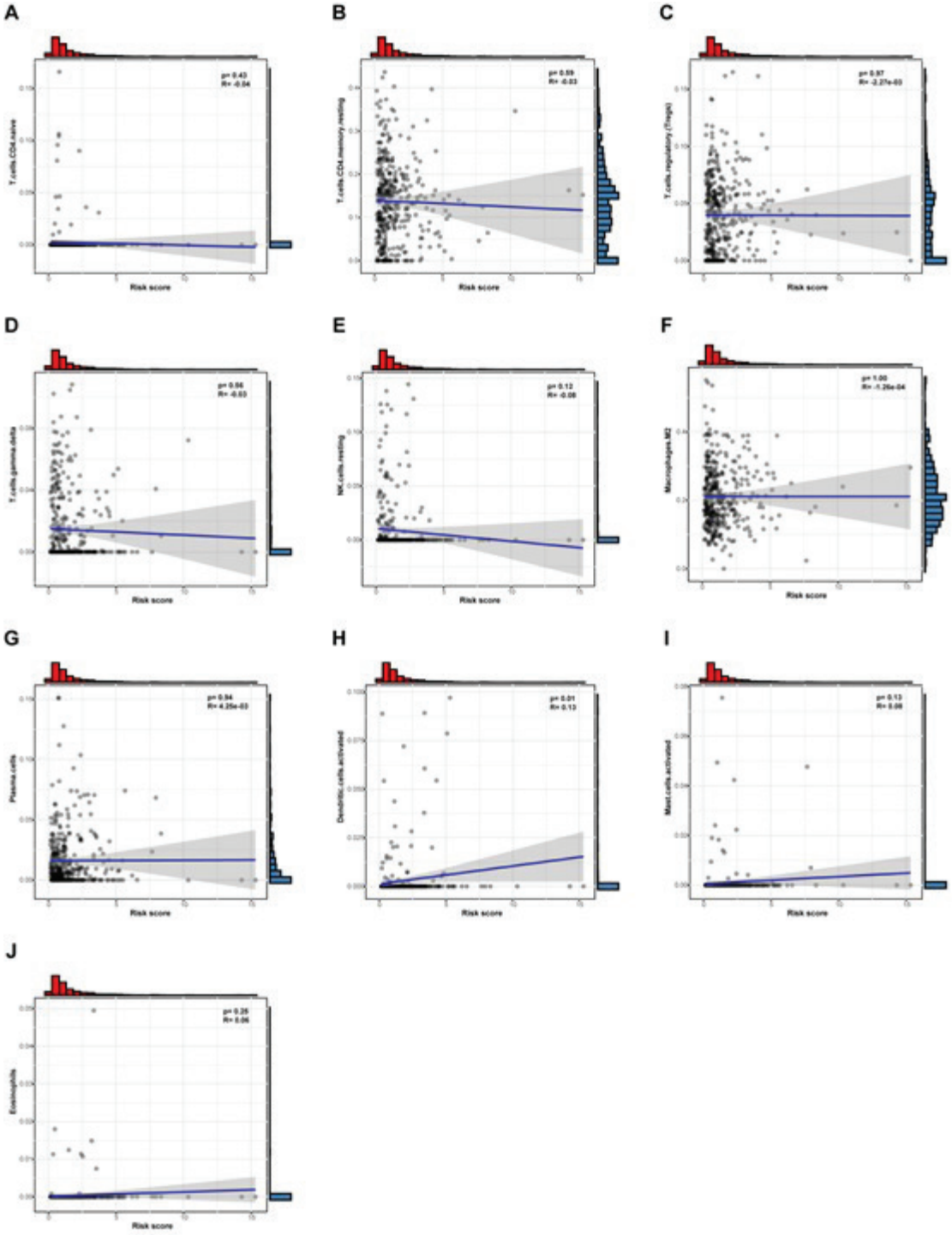

Supplementary Figure 3: Establishment of the PMRG_score model and its relationship with immune cells

Supplementary Table 3: DEGs between cluster 1 and cluster 2.

	logFC	AveExpr	t	P.Value	FDR	B	significant
TMSB10	2.420214702	9.638578672	13.82735811	1.94E-31	5.67E-27	59.78010306	up
TIMP1	2.554684522	6.39161303	11.10226765	6.98E-23	2.15E-19	40.12108113	up
PKM	2.055848177	4.029646491	10.92853321	2.38E-22	5.57E-19	38.89781657	up
IER3	1.953459964	3.874590183	10.80039919	5.88E-22	1.18E-18	37.99908656	up
CXCL1	2.215458804	1.536324531	10.62737775	1.98E-21	2.90E-18	36.7904556	up
SEL1L3	1.746853303	2.053998912	10.51559075	4.32E-21	5.87E-18	36.01274126	up
S100A6	2.449470719	5.550525812	10.35442973	1.33E-20	1.58E-17	34.89612958	up
TMSB4X	1.50455473	8.113693528	10.12783886	6.36E-20	5.99E-17	33.33589948	up
GOLM1	1.832403717	3.811896918	10.10010349	7.70E-20	6.92E-17	33.14573826	up
CXCL8	1.945320284	1.748001609	10.07117043	9.40E-20	8.19E-17	32.9475606	up
TESC	2.213399473	2.670205688	9.778737613	6.96E-19	4.15E-16	30.95613552	up
QSOX1	2.040894415	2.884436848	9.77455967	7.17E-19	4.23E-16	30.9278424	up
PFKP	1.571103559	1.720170838	9.763743587	7.71E-19	4.46E-16	30.85461698	up
PFKFB3	1.622412078	2.247451112	9.701907417	1.17E-18	6.23E-16	30.4365782	up
S100A11	2.092836932	6.118854732	9.620426005	2.04E-18	1.01E-15	29.88729964	up
TGFB1	1.523587167	3.154057356	9.480305004	5.26E-18	2.34E-15	28.94701383	up
MMP7	2.051121769	1.411511127	9.47451124	5.47E-18	2.40E-15	28.90825399	up
RGS2	1.645572792	2.58854157	9.471041923	5.60E-18	2.44E-15	28.88504912	up
SLC1A5	1.652664666	2.607666884	9.436897385	7.04E-18	2.94E-15	28.65685469	up
PHLDA2	1.611117639	2.406407973	9.14399308	4.98E-17	1.57E-14	26.71352012	up
BICC1	1.534361283	1.636344346	9.126639777	5.59E-17	1.73E-14	26.59920945	up
NNMT	2.138145018	4.05940046	8.967429349	1.60E-16	4.43E-14	25.55493147	up
SPHK1	1.756023514	1.868345168	8.952210856	1.77E-16	4.76E-14	25.45554216	up
CTHRC1	1.571764603	1.785440768	8.740325885	7.08E-16	1.60E-13	24.07982374	up
CYBA	1.759797609	3.556846244	8.618350686	1.56E-15	3.19E-13	23.29489755	up
SELM	1.530144343	2.911979478	8.218206354	2.02E-14	3.09E-12	20.75822446	up
COL1A1	1.906867424	4.385708354	7.818379492	2.46E-13	2.68E-11	18.28663597	up
SPP1	3.083993441	5.374570945	7.473616388	2.01E-12	1.74E-10	16.21057876	up
COL1A2	1.590618942	3.682692905	7.381806578	3.48E-12	2.81E-10	15.66686694	up
TRNP1	1.634406007	2.72753021	7.367489564	3.80E-12	3.02E-10	15.58243675	up
B3GNT3	1.554103088	2.200316589	7.093445263	1.92E-11	1.27E-09	13.98541598	up
LY6E	1.651915443	4.360238523	6.928207008	5.00E-11	2.95E-09	13.0405262	up
S100A9	1.681557772	3.427175632	6.899093717	5.91E-11	3.45E-09	12.87549684	up
LGALS3BP	1.582287521	6.248552878	6.689986528	1.95E-10	1.00E-08	11.70326906	up
SPINT1	1.835351396	2.192259454	6.630752267	2.72E-10	1.35E-08	11.37546805	up
CA9	1.760463821	1.551662206	6.598680154	3.25E-10	1.58E-08	11.19878087	up
CD24	1.959870472	4.555485768	6.420253785	8.75E-10	3.76E-08	10.22623742	up
COL3A1	1.600328896	4.491443628	6.359862628	1.22E-09	5.03E-08	9.901130664	up
CRP	2.891686872	5.728193309	6.356735226	1.24E-09	5.11E-08	9.884351557	up
LUM	1.552004163	2.405540082	6.310896271	1.59E-09	6.35E-08	9.6390628	up
KRT23	1.717228025	1.983586717	6.027197442	7.28E-09	2.39E-07	8.148384298	up
LCN2	1.991649691	3.889371635	5.727927214	3.45E-08	9.37E-07	6.628895723	up
KRT19	1.70564848	1.935335412	5.725706008	3.48E-08	9.46E-07	6.617827992	up
IGHA1	1.830336073	4.163380311	5.572226835	7.57E-08	1.87E-06	5.860754922	up
CCL20	1.589239214	3.510130754	5.512902938	1.02E-07	2.42E-06	5.572226022	up
NTS	1.808350937	1.243216191	5.272998497	3.29E-07	6.82E-06	4.429279348	up
S100P	1.800837593	2.604989273	5.180354322	5.13E-07	1.01E-05	3.998345148	up
IGHG2	1.783504404	3.263153654	5.057123582	9.18E-07	1.67E-05	3.434351	up
NQO1	1.780037879	3.437488235	5.048674216	9.55E-07	1.73E-05	3.396069941	up
SPINK1	2.159783285	4.822732665	4.886647714	2.02E-06	3.32E-05	2.671786007	up
DEFB1	1.916473717	5.70389645	4.474373358	1.25E-05	0.000161147	0.915087555	up
PTGDS	1.548836578	2.640891993	4.291221656	2.70E-05	0.000315969	0.175711025	up
IGKC	1.785521932	4.273833758	4.257202616	3.11E-05	0.000356075	0.041229917	up
IGLC2	1.562798314	3.70086428	4.204301104	3.86E-05	0.000429484	-0.166101268	up
IGHG1	1.788104371	4.222508508	3.995234861	8.91E-05	0.000892142	-0.963852333	up
Metazoa_SRP	1.50428403	10.70009484	3.798923744	0.000189732	0.001692314	-1.680973463	up
CPS1	-4.717813832	4.760624521	-18.9549609	1.47E-47	8.57E-43	96.91329903	down
BHMT	-3.373682863	4.458612289	-12.55512793	2.07E-27	4.03E-23	50.51930084	down
ALDH6A1	-1.829691723	4.081727108	-12.12883407	4.52E-26	6.60E-22	47.44221324	down
CYP7A1	-3.130139937	3.190788893	-12.06459563	7.18E-26	8.39E-22	46.98011889	down
ACADSB	-1.763620567	4.505385608	-11.82131565	4.13E-25	4.02E-21	45.23438477	down
EHHADH	-2.078753508	4.598463282	-11.66957584	1.23E-24	8.96E-21	44.14921676	down
NR1I3	-2.270195423	3.026847127	-11.55321774	2.82E-24	1.83E-20	43.31915568	down
DMGDH	-1.888251179	3.193656195	-11.4804327	4.75E-24	2.52E-20	42.80089258	down
TAT	-3.489242954	4.311518864	-11.4182068	7.40E-24	3.60E-20	42.35842355	down
SORD	-1.772212356	4.282324006	-11.24751951	2.49E-23	9.70E-20	41.14772149	down

KLF15	-1.645252863	4.355388925	-11.09184914	7.52E-23	2.19E-19	40.04757745	down
SLC6A1	-2.190342696	3.953637883	-11.05804295	9.55E-23	2.66E-19	39.80919841	down
ETNK2	-2.175053436	3.977445477	-11.01727443	1.27E-22	3.38E-19	39.52198655	down
RTP3	-2.698935957	3.143311979	-10.87211518	3.55E-22	7.97E-19	38.50172901	down
CTH	-2.006427323	3.133953288	-10.85809631	3.92E-22	8.47E-19	38.40339857	down
CDO1	-2.500580345	5.145343473	-10.8332881	4.66E-22	9.73E-19	38.22947921	down
MIR621	-2.086391949	5.343156612	-10.76452011	7.56E-22	1.42E-18	37.74797995	down
MASP2	-2.484180451	4.047728529	-10.72673596	9.86E-22	1.69E-18	37.48380612	down
SLC25A15	-1.659583922	3.305871033	-10.67984247	1.37E-21	2.29E-18	37.1563275	down
PCK2	-1.857750777	5.658846857	-10.65296167	1.65E-21	2.61E-18	36.96880131	down
SLC27A5	-2.541192159	4.099886741	-10.62687621	1.99E-21	2.90E-18	36.78696072	down
ACOX2	-1.772051388	4.05058504	-10.59892152	2.41E-21	3.44E-18	36.59224115	down
PAH	-2.20261372	5.745366703	-10.52310994	4.10E-21	5.70E-18	36.06497255	down
CPN2	-2.236687379	5.252161489	-10.45740633	6.48E-21	8.41E-18	35.60896883	down
PIPOX	-2.072832192	5.382016092	-10.43566931	7.54E-21	9.57E-18	35.45830775	down
ABAT	-1.777770146	3.863621593	-10.31929797	1.69E-20	1.90E-17	34.6534643	down
CYP8B1	-3.363978453	3.714046801	-10.25656979	2.61E-20	2.64E-17	34.22086606	down
DCXR	-1.927216551	7.076855415	-9.980392932	1.75E-19	1.44E-16	32.32709185	down
ADH4	-3.544411759	5.236347563	-9.946603345	2.21E-19	1.74E-16	32.0966553	down
HNF4A.AS1	-1.611206424	1.97980326	-9.93030222	2.47E-19	1.83E-16	31.98558743	down
CYP4F3	-1.721845449	4.202522875	-9.895112516	3.15E-19	2.21E-16	31.74604975	down
ACOT12	-1.814972672	2.846851734	-9.89273926	3.20E-19	2.22E-16	31.72990617	down
NR1I2	-1.602014993	1.948538483	-9.874190759	3.63E-19	2.41E-16	31.60378315	down
PFKFB1	-1.756049581	2.246873862	-9.826479265	5.03E-19	3.19E-16	31.2797669	down
KNG1	-2.539722462	8.239244581	-9.809233661	5.66E-19	3.55E-16	31.16279381	down
HFE2	-2.579784793	5.244781849	-9.801244428	5.97E-19	3.67E-16	31.10863082	down
ARG1	-2.695818153	5.668763399	-9.767837895	7.50E-19	4.38E-16	30.88233203	down
SLC27A2	-1.870404786	4.444242669	-9.756413604	8.11E-19	4.64E-16	30.80501016	down
BDH1	-1.559153637	3.477484447	-9.753650378	8.26E-19	4.68E-16	30.78631327	down
SLC2A2	-2.342110222	5.827570069	-9.709493952	1.12E-18	5.98E-16	30.48781153	down
SERPINC1	-3.132553625	9.046355092	-9.671340511	1.45E-18	7.47E-16	30.23031089	down
CCL16	-2.628189978	4.204533992	-9.657784465	1.58E-18	8.12E-16	30.13891474	down
RGN	-1.709806791	4.844295188	-9.636556989	1.83E-18	9.29E-16	29.99589754	down
SLC10A1	-3.036158258	3.862244015	-9.624284381	1.99E-18	9.92E-16	29.91326872	down
SLC38A4	-2.018166374	4.813225729	-9.603154102	2.29E-18	1.13E-15	29.77110008	down
PROZ	-1.63093269	2.680869702	-9.567342148	2.92E-18	1.38E-15	29.53043227	down
PLG	-2.387747763	6.38828041	-9.495025032	4.76E-18	2.14E-15	29.04553283	down
OTC	-2.582864739	4.346484645	-9.454313368	6.26E-18	2.65E-15	28.77320705	down
RNU1.70P	-2.389724043	6.219344817	-9.412576664	8.29E-18	3.39E-15	28.49452031	down
ACSM2A	-2.02775372	3.368844167	-9.399550695	9.05E-18	3.67E-15	28.40764623	down
HPD	-3.514634616	6.133575905	-9.393210443	9.44E-18	3.78E-15	28.36537914	down
GPLD1	-1.713211943	1.944747411	-9.364206369	1.15E-17	4.43E-15	28.17217487	down
DAO	-1.850032589	2.92032754	-9.348622368	1.27E-17	4.86E-15	28.06846797	down
F12	-2.264832015	6.308210262	-9.345625702	1.30E-17	4.92E-15	28.04853429	down
NAGS	-1.690572146	2.869303948	-9.325335831	1.49E-17	5.53E-15	27.91363731	down
F13B	-2.041751161	4.508000385	-9.271540004	2.13E-17	7.64E-15	27.55657302	down
ADH6	-1.890419648	4.643268785	-9.263663877	2.25E-17	7.95E-15	27.50436931	down
SLCO1B1	-2.185390417	4.672625542	-9.244086516	2.56E-17	8.95E-15	27.37469036	down
SLC38A3	-2.096020727	6.386533329	-9.218403687	3.04E-17	1.03E-14	27.20474673	down
PBLD	-1.510591797	3.477841712	-9.189807551	3.67E-17	1.20E-14	27.01576426	down
SULT2A1	-2.829959093	6.339392822	-9.179233049	3.94E-17	1.28E-14	26.94594488	down
SEC14L2	-1.985983672	3.56044414	-9.178083188	3.97E-17	1.28E-14	26.93835488	down
SPP2	-2.698015132	4.329755375	-9.137670303	5.20E-17	1.61E-14	26.67185941	down
G6PC	-2.506838424	5.849815843	-9.010782019	1.20E-16	3.43E-14	25.838476	down
LECT2	-2.493569439	3.574702397	-8.956783009	1.72E-16	4.66E-14	25.48539408	down
GLYATL1	-1.757161335	2.656308471	-8.937330209	1.95E-16	5.13E-14	25.35843307	down
ABCB11	-1.744247569	1.871643877	-8.927335209	2.08E-16	5.43E-14	25.29324817	down
ACSM2B	-1.959602365	3.885133632	-8.877519292	2.89E-16	7.27E-14	24.96885705	down
ETNPPL	-1.911486363	2.787020599	-8.859885142	3.24E-16	8.06E-14	24.85422633	down
FETUB	-2.46728043	3.626643517	-8.844108409	3.60E-16	8.90E-14	24.75175866	down
MAT1A	-1.839807147	6.643643829	-8.804485534	4.66E-16	1.11E-13	24.49478633	down
SLC6A12	-1.565643689	2.495433568	-8.801482103	4.75E-16	1.12E-13	24.47532955	down
HGD	-1.652199543	5.911582075	-8.784035004	5.33E-16	1.25E-13	24.36236525	down
TTR	-2.521698581	8.277150038	-8.759187275	6.26E-16	1.46E-13	24.20166517	down
BHMT2	-1.773395406	5.624811272	-8.716349089	8.28E-16	1.82E-13	23.92511634	down
SELENBP1	-1.536100462	5.485331674	-8.660847749	1.19E-15	2.50E-13	23.56777437	down
AQP9	-2.919210751	5.095176545	-8.618292542	1.56E-15	3.19E-13	23.29452464	down
GYS2	-1.937399818	2.289275534	-8.595087733	1.82E-15	3.59E-13	23.14579816	down
AGXT	-2.416675632	6.644318874	-8.547387577	2.47E-15	4.70E-13	22.84068464	down

F7	-1.627216872	4.821043417	-8.541103125	2.57E-15	4.83E-13	22.80054787	down
HLF	-1.706209794	3.041206919	-8.531250204	2.74E-15	5.11E-13	22.7376495	down
ABCB4	-1.748048918	3.010617235	-8.49280122	3.51E-15	6.51E-13	22.49254242	down
AHSG	-3.004072088	9.074177423	-8.483528908	3.73E-15	6.84E-13	22.43351426	down
ASPDH	-1.942661629	3.295610274	-8.474749441	3.94E-15	7.19E-13	22.37765293	down
CPB2	-1.736891264	7.383406244	-8.459830136	4.34E-15	7.81E-13	22.28279116	down
ADH1A	-2.353054103	6.053143131	-8.456016027	4.45E-15	7.96E-13	22.25855312	down
MTND4P20	-1.795320481	2.413062048	-8.443900351	4.80E-15	8.53E-13	22.18159597	down
KHK	-1.582996582	5.282664309	-8.443379942	4.82E-15	8.53E-13	22.17829163	down
LINC01018	-2.060345582	1.993100931	-8.4036569	6.22E-15	1.07E-12	21.92636982	down
APOA5	-2.283236925	5.305447062	-8.379447915	7.26E-15	1.22E-12	21.77312929	down
SLC47A1	-1.546477213	3.520222609	-8.372739657	7.57E-15	1.26E-12	21.73070599	down
HAO1	-2.061237573	5.475132478	-8.371896295	7.61E-15	1.26E-12	21.72537374	down
RP11.468N14.3	-1.687355013	2.304892961	-8.303504233	1.18E-14	1.88E-12	21.29386305	down
CYP4A22	-1.814849662	3.268488453	-8.258840688	1.56E-14	2.43E-12	21.01303846	down
TTPA	-1.653981617	3.454403137	-8.247374834	1.68E-14	2.60E-12	20.94107161	down
GNMT	-2.353742278	4.081126312	-8.223096126	1.96E-14	3.01E-12	20.78885341	down
AZGP1	-1.963240967	6.890471693	-8.220737976	1.99E-14	3.05E-12	20.77408107	down
CES2	-1.76224022	5.72736086	-8.193151267	2.37E-14	3.55E-12	20.60143051	down
F9	-2.3326939	4.046771519	-8.180940974	2.56E-14	3.81E-12	20.52510901	down
DPYS	-2.010177957	4.645462377	-8.172203945	2.70E-14	4.01E-12	20.47053384	down
CYP4A11	-2.110346436	4.909496933	-8.169809422	2.74E-14	4.06E-12	20.45558194	down
MTTP	-1.755314569	4.019338901	-8.139357053	3.32E-14	4.77E-12	20.26563092	down
UGT2B10	-2.34607368	4.869900319	-8.133814369	3.44E-14	4.87E-12	20.23109761	down
GLYAT	-2.20753358	2.62585846	-8.124546347	3.65E-14	5.11E-12	20.17338144	down
HPR	-2.272721326	5.777034163	-8.120799682	3.74E-14	5.21E-12	20.15005907	down
F10	-1.54762192	6.007069925	-8.108737114	4.03E-14	5.54E-12	20.07501007	down
CYP2C9	-2.485310916	5.132065686	-8.074963724	4.98E-14	6.73E-12	19.86519753	down
HMGCS2	-2.152906171	7.777925388	-8.02701551	6.73E-14	8.75E-12	19.5681249	down
CYP27A1	-1.537373699	6.670201531	-8.002698739	7.83E-14	1.00E-11	19.41782677	down
EPHX1	-1.586938717	9.33590551	-8.002523276	7.84E-14	1.00E-11	19.41674315	down
SERPIND1	-2.083832593	7.716666669	-7.986739839	8.65E-14	1.09E-11	19.31932031	down
PROC	-1.544270748	6.296061776	-7.968669279	9.68E-14	1.20E-11	19.20790741	down
RBP4	-1.852747228	10.63984208	-7.931095621	1.22E-13	1.48E-11	18.97668621	down
AKR1D1	-1.83874699	2.725354283	-7.91829868	1.32E-13	1.58E-11	18.8980716	down
CTC.505O3.2	-1.890319356	2.234270365	-7.905426428	1.43E-13	1.70E-11	18.81906406	down
SLC1A2	-1.510823119	1.507160471	-7.903956789	1.45E-13	1.71E-11	18.81004814	down
HSD17B6	-2.242135572	6.003690087	-7.80744884	2.63E-13	2.84E-11	18.22000762	down
TTC36	-1.776693567	1.770846083	-7.79425175	2.85E-13	3.06E-11	18.13963292	down
INSIG1	-1.557037008	5.800925923	-7.771791839	3.27E-13	3.46E-11	18.00301826	down
ABCG8	-1.682503557	3.656644477	-7.742595243	3.92E-13	4.09E-11	17.82575574	down
PKLR	-1.92511232	4.92658537	-7.731673157	4.19E-13	4.35E-11	17.75953995	down
DIO1	-1.966846371	4.49452533	-7.699105901	5.11E-13	5.19E-11	17.56241074	down
TF	-2.106969893	8.911140449	-7.670360523	6.09E-13	6.03E-11	17.38880518	down
TFR2	-1.599086329	6.313884115	-7.641427245	7.27E-13	7.02E-11	17.21443635	down
LINC01485	-2.034964267	3.184783869	-7.565197915	1.16E-12	1.07E-10	16.75683566	down
RBP5	-1.678491398	5.039697764	-7.537973786	1.36E-12	1.23E-10	16.59404957	down
BAAT	-1.709137891	6.511718288	-7.534633	1.39E-12	1.24E-10	16.57409675	down
APOC3	-2.48432949	10.50032484	-7.526225786	1.46E-12	1.30E-10	16.52390736	down
A1BG	-1.554332129	3.421507295	-7.446797272	2.36E-12	2.00E-10	16.05134409	down
RP11.115C10.1	-1.781360566	1.63914039	-7.415986552	2.84E-12	2.34E-10	15.86882424	down
PDK4	-1.68794363	3.957906298	-7.414354617	2.87E-12	2.36E-10	15.85916921	down
ACSM5	-1.76665244	3.104452687	-7.411015317	2.93E-12	2.40E-10	15.8394168	down
GBP7	-1.53465093	2.19103799	-7.391315889	3.29E-12	2.67E-10	15.72299877	down
FNDC5	-1.783264998	1.90855047	-7.360743644	3.95E-12	3.14E-10	15.54268843	down
CYP2A6	-3.112686699	4.577605634	-7.326211626	4.85E-12	3.78E-10	15.33955798	down
CYP2D6	-1.967924085	5.232903855	-7.300234212	5.67E-12	4.34E-10	15.18712463	down
RP11.372E1.4	-1.604182201	2.219903432	-7.295953967	5.81E-12	4.44E-10	15.16203959	down
IGSF23	-1.508562201	2.509106108	-7.290933944	5.99E-12	4.56E-10	15.1326302	down
ALDOB	-2.5576432	8.496546983	-7.287335324	6.12E-12	4.64E-10	15.11155545	down
HULC	-2.219674862	6.63639375	-7.241935642	8.00E-12	5.86E-10	14.84621704	down
LINC00844	-2.1555305	2.207778321	-7.207009215	9.84E-12	7.05E-10	14.64277146	down
ADH1B	-2.406315474	5.802117333	-7.203581081	1.00E-11	7.17E-10	14.6228348	down
C8A	-1.690895725	5.171864625	-7.126620787	1.58E-11	1.08E-09	14.17678813	down
CYP4F2	-1.746908571	3.538805833	-7.116615628	1.67E-11	1.13E-09	14.11901578	down
PCK1	-2.182834341	4.295705247	-7.102051977	1.82E-11	1.21E-09	14.03501077	down
SERPINA4	-1.823132213	5.625390858	-7.088165225	1.98E-11	1.30E-09	13.95500899	down
UPB1	-1.662557762	3.809368449	-7.04262021	2.58E-11	1.64E-09	13.69330359	down
ALDH1L1	-1.892837641	3.725962452	-6.987754271	3.54E-11	2.18E-09	13.37943386	down

CYP2B6	-1.626358252	3.216005314	-6.984458071	3.61E-11	2.22E-09	13.36062625	down
GSTA1	-2.526917743	7.47159412	-6.933901212	4.84E-11	2.87E-09	13.07285526	down
APOB	-1.505615511	7.678465823	-6.923864315	5.13E-11	3.02E-09	13.01588167	down
ANGPTL3	-1.629955194	5.661478115	-6.746488846	1.41E-10	7.52E-09	12.0177201	down
INHBC	-1.505420951	3.709005656	-6.708003301	1.76E-10	9.13E-09	11.80335075	down
TMPRSS6	-1.567244743	4.848446149	-6.707039457	1.77E-10	9.17E-09	11.79799224	down
ITIH1	-1.701978663	7.43466678	-6.646936151	2.48E-10	1.25E-08	11.46483971	down
HPX	-1.759692181	7.737080226	-6.532495321	4.70E-10	2.16E-08	10.8359564	down
PRAP1	-1.933399307	7.133379734	-6.518691914	5.08E-10	2.31E-08	10.76059254	down
FBP1	-1.514126829	5.6208248	-6.498445168	5.68E-10	2.56E-08	10.6502417	down
RDH16	-1.747246436	3.572026028	-6.49301567	5.85E-10	2.63E-08	10.6206883	down
F2	-1.659947716	8.208682764	-6.454419014	7.25E-10	3.17E-08	10.41107925	down
SERPINF2	-1.542335213	8.047734335	-6.373605445	1.13E-09	4.71E-08	9.97492994	down
CYP3A4	-3.067091558	4.326405533	-6.364837501	1.19E-09	4.92E-08	9.927833359	down
APOA2	-2.302775472	12.42238671	-6.270859709	1.98E-09	7.67E-08	9.425817673	down
FMO3	-1.787327785	5.315730976	-6.21542964	2.67E-09	9.99E-08	9.132125801	down
CYP2A7	-1.836626112	1.682123333	-6.187182179	3.11E-09	1.14E-07	8.98315299	down
SLC22A1	-2.081511841	3.416077794	-6.114530874	4.58E-09	1.61E-07	8.60217297	down
UROC1	-1.545950624	2.160136063	-6.05756414	6.20E-09	2.08E-07	8.30564936	down
AKR1C4	-1.644550161	5.503659223	-6.042199933	6.73E-09	2.23E-07	8.226010388	down
APOM	-1.591048205	6.49093321	-6.040774046	6.78E-09	2.24E-07	8.218626678	down
SLC39A5	-1.656593042	4.21959837	-6.002307344	8.30E-09	2.68E-07	8.019899206	down
UGT1A4	-1.819545639	2.553988404	-5.993765577	8.69E-09	2.80E-07	7.97589275	down
HAO2	-1.644943337	2.468097191	-5.980121807	9.33E-09	2.98E-07	7.905693634	down
SLC22A7	-1.972609832	4.759059984	-5.888578131	1.51E-08	4.53E-07	7.437647066	down
HSD11B1	-2.31059265	4.790368162	-5.882476141	1.55E-08	4.66E-07	7.40663285	down
AFM	-1.660667596	4.708547131	-5.866893046	1.69E-08	5.01E-07	7.327534691	down
HRG	-2.245549585	6.504846185	-5.814683815	2.21E-08	6.37E-07	7.063631214	down
GSTA2	-2.179451299	4.457268512	-5.751496068	3.05E-08	8.44E-07	6.74652703	down
FTCD	-1.539015388	5.25461707	-5.737097058	3.29E-08	9.01E-07	6.67462009	down
PON1	-1.686484598	5.208299494	-5.583447444	7.16E-08	1.78E-06	5.915586687	down
CFHR5	-1.60482902	3.702694045	-5.227623803	4.10E-07	8.28E-06	4.217482219	down
APOH	-1.601028132	10.56853943	-5.157116012	5.73E-07	1.11E-05	3.891180429	down
HP	-1.655713606	8.080953977	-5.09392297	7.73E-07	1.44E-05	3.601661052	down
CYP2C8	-1.644686338	4.904020281	-4.961869584	1.43E-06	2.45E-05	3.005712744	down
HSD17B13	-1.816308484	2.900828143	-4.868066332	2.20E-06	3.56E-05	2.589925309	down
NOTUM	-1.610037752	2.712749548	-4.440532361	1.44E-05	0.000182921	0.77653617	down
THRSP	-1.589956404	2.599841856	-4.31148288	2.48E-05	0.000293425	0.256233322	down
SDS	-1.539498085	3.608562272	-4.256482601	3.12E-05	0.000356922	0.038393358	down
APOA1	-1.615761448	10.66404778	-4.145977149	4.89E-05	0.000529541	-0.392138063	down

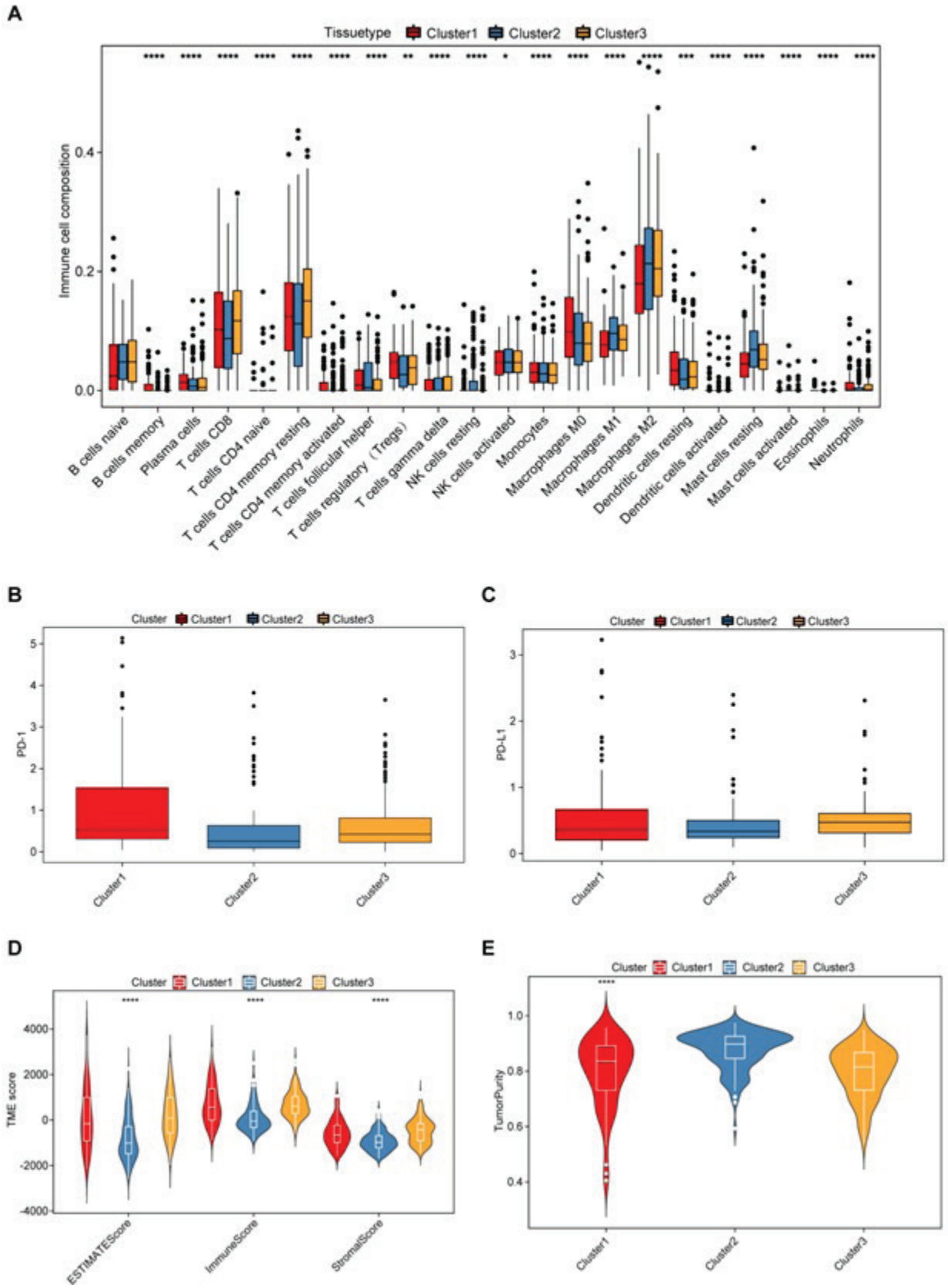

Figure 3: Correlations of tumor immune cell microenvironments and Three polyamine subtypes.

(A) Abundance of 22 infiltrating immune cell types in the three polyamine subtypes by CIBERSORT. (B-C) Expression levels of PD-1 and PD-L1 in the three polyamine subtypes. (D) Correlations between the three polyamine subtypes and TME score by ESTIMATE. (E) The TumorPurity in the three polyamine subtypes by ESTIMATE. TME, tumor microenvironment.

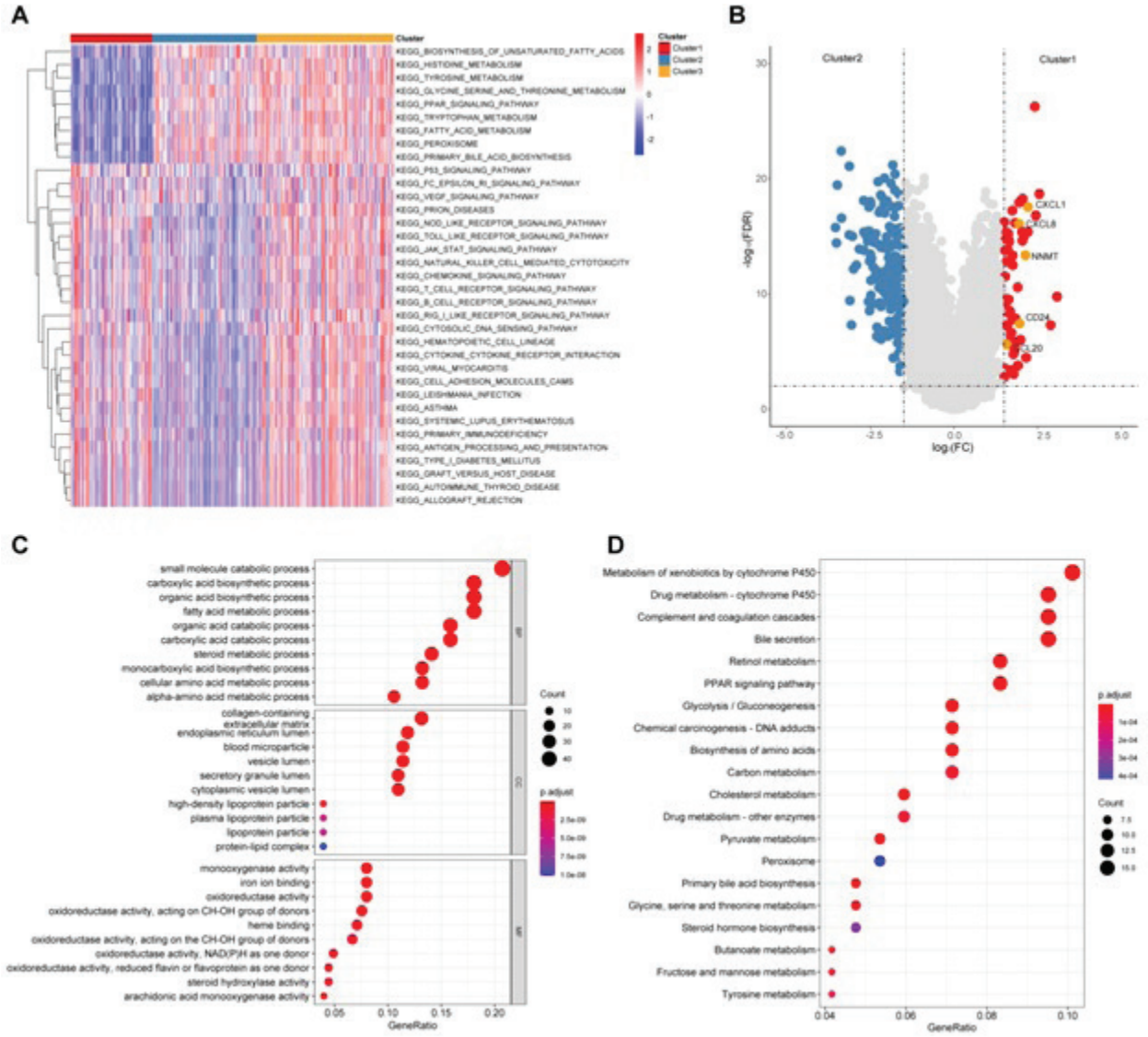

Figure 4:. GSVA of biological pathways between two distinct subtypes.
(A) GSVA of biological pathways between three distinct subtypes. (B) The volcano of the differential expression of genes between cluster1 and cluster2 in the TCGA-LIHC cohort. (C-D) GO and KEGG enrichment analyses of polyamine-related DEGs among two polyamine subtypes. GSVA, gene set variation analysis; GO, Gene Ontology; KEGG, Kyoto Encyclopedia of Genes and Genomes; DEGs, differentially expressed genes.

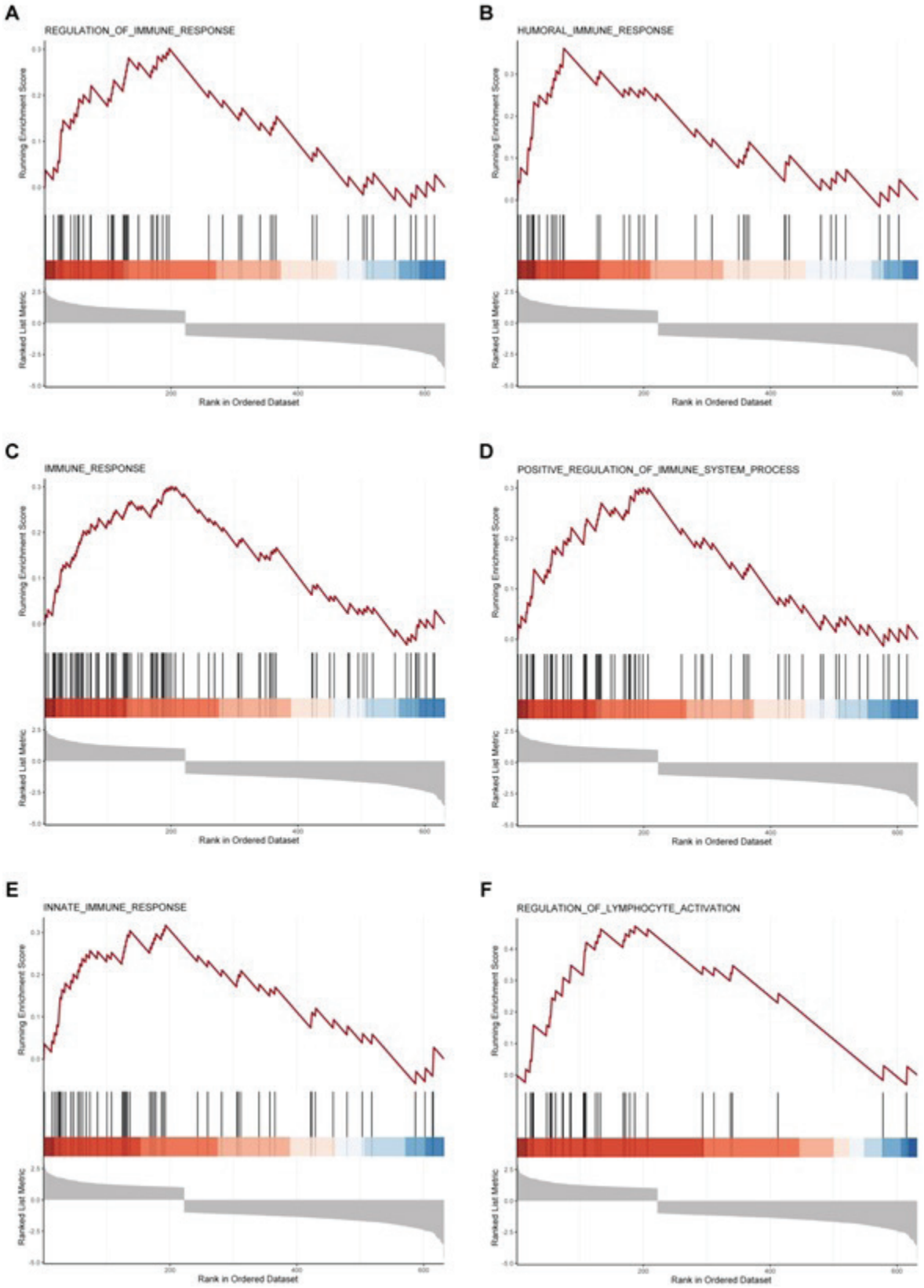

Figure 5: GSEA between two polyamine-ralated subtypes in the TCGA cohort.

5.5. Construction of the PMRG-score and evaluation of TME and checkpoints based on the PMRG-score

We set up PMRG_score based on the above-mentioned polyamine-related DEGs. First of all, we conducted a univariate Cox regression analysis. To find the best prognostic indicators, the DEGs related to the polyamine subtype have further carried out LASSO and multivariate Cox analyses, and finally got 12 genes(SLC1A5, S100A9, SPP1, ADH4, PON1, FTCD, TRNP1, MTND4P20, EHHADH, PLG, TMSB10, PCK2). At the same time, the risk score was calculated. Patients with PMRG scores lower than the mid-level risk score were attributed to low-risk groups (N = 182), and patients with PMRG scores higher than the median risk score were attributed to high-risk groups (n = 183). According to the risk distribution diagram of PMRG_Score, we found that with the increase of PMRG_Score, the reduction of the patient's survival time and the increase in recurrence rate (Figure 6A, B). Kaplan-Meier survival curve displayed that, compared to patients with high scores, low scores patients have a higher survival rate (figure 6C). In addition, the AUC value of the 1 -year survival rate of PMRG_Score is 0.809, the AUC value of the 3 -year survival rate is 0.747, and the AUC value of the 5 -year survival rate is 0.730. We also evaluated the immune checkpoints of high-risk patients and low-risk patients. The results showed that 25 immune checkpoints were expressed in differences between high-risk and low-risk patients. Compared with low-risk patients, the immune checkpoints of high-risk patients were raised, including PD-1, PD-L1, and CTLA4. In the end, we evaluated the relationship between PMRG_Score and immune cell infiltration based on the cibersort algorithm. The figure shows that PMRG_Score is negatively correlated with naive B cells, CD8+T cells, resting mast cells, activated NK cells, and M1 macrophages. PMRG_Score positively correlates with memory B cells, CD4+ memory activated T cells, follicular helper T cells, monocytes, M0 macrophages, resting dendritic cells, and neutrophils (Figure 7).

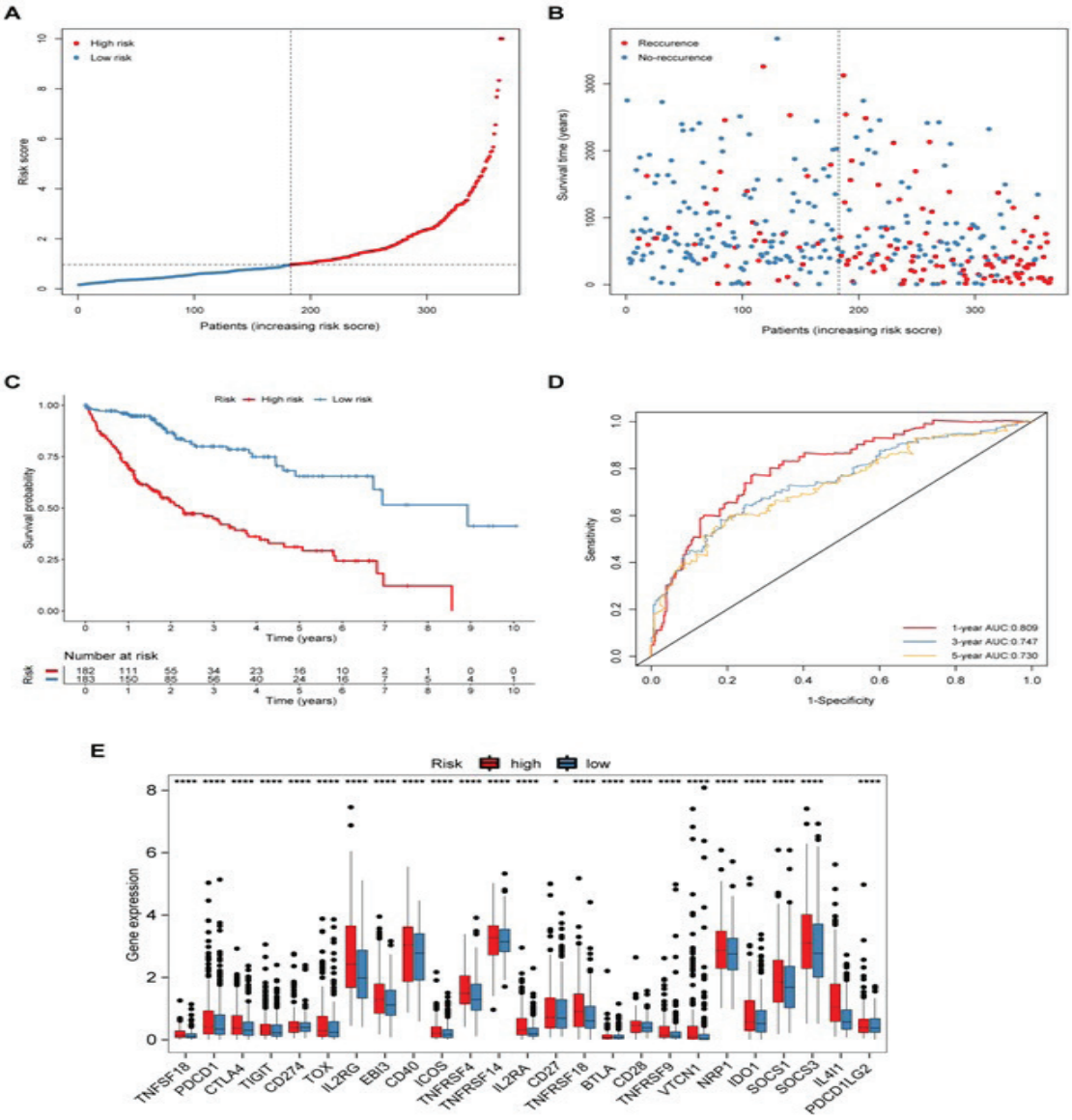

Figure 6: Construction of the PMRG_score

(A-B) Ranked dot and scatter plots showing the PMRG_score distribution and patient survival status. (C) Kaplan–Meier analysis of the RFS between the two groups. (D) ROC curves to predict the sensitivity and specificity of 1-, 3-, and 5- survival according to the PMRG_score. (E) Expression of immune checkpoints in the high and low-risk populations. PMRG, polyamine metabolism-related gene.

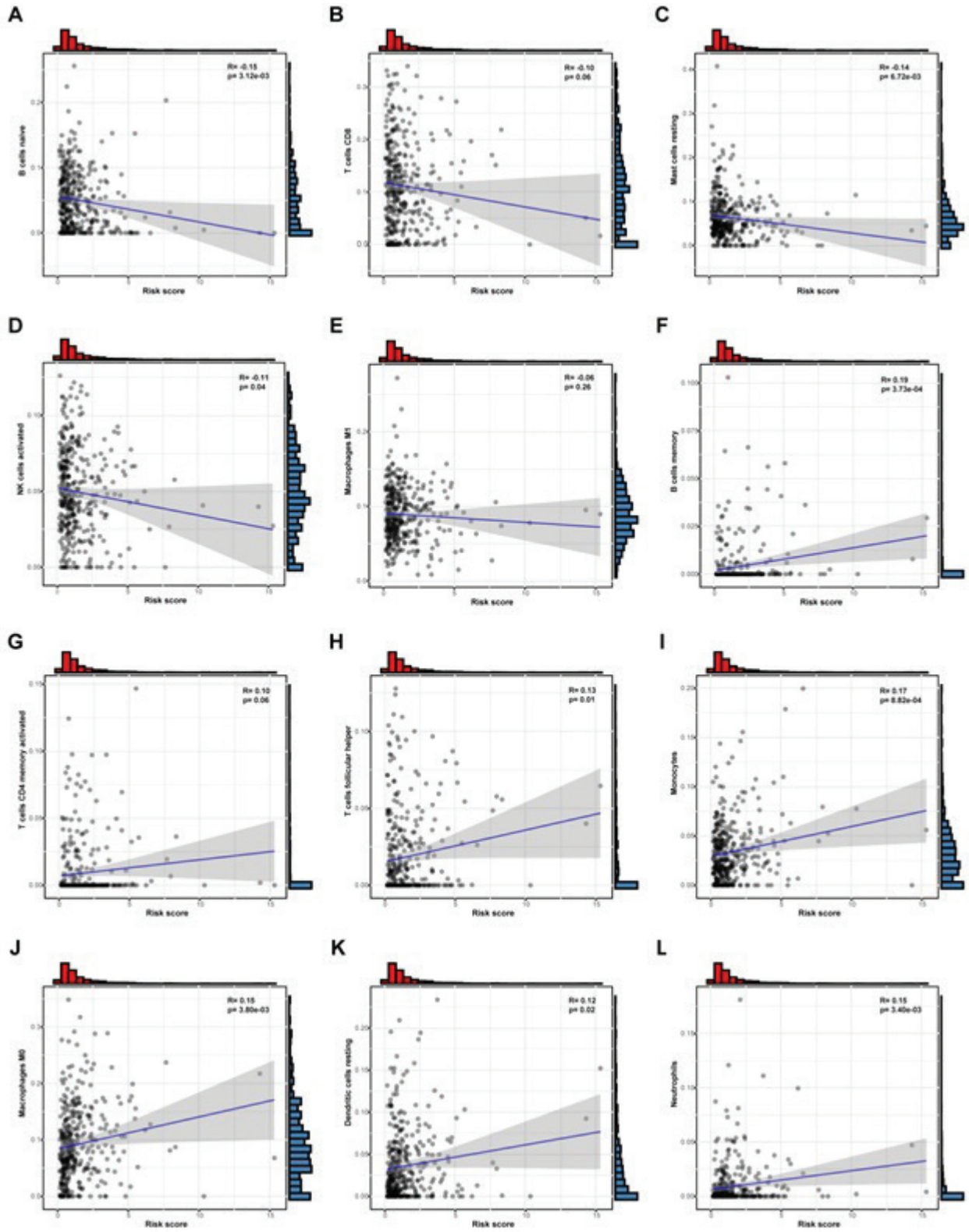

Figure 7: Establishment of the PMRG_score model and its relationship with immune cells

(A-E) B cells naïve, T cells CD8, Mast cells resting, NK cells activated and Macrophages M1. (F-L) B cells memory, T cells CD4 memory active, T cells follicular helper, Monocytes, Macrophages M0, Dendritic resting and Neutrophils.

6. Discussion

HCC is one of the leading causes of cancer-related death. With the popularity of obesity, the incidence of non-alcoholic fatty liver disease and the chance of subsequent development of HCC are rising. The surgery treatments can cure the early stages of liver cancer, but there is still a high recurrence rate, and the treatment plan for patients with advanced liver cancer is also limited in availability and effectiveness [28]. Tumor immune function affects patient prognosis, while standard treatments have a poor prognosis. Therefore, immunotherapy has recently been shown as an emerging antitumor method in treating liver cancer [29].

Polyamine plays a vital role in cell proliferation, autophagy, and regulating ion channels. Its steady-state is maintained through polyamine and transshipment synthesis and decomposition metabolism. The occurrence and development of many cancers are accompanied by the elevation of polyamine levels, such as colon cancer and breast cancer. Studies have shown that polyamine can be used as a colon cancer biomarker. The lipid-droplet-associated protein ABHD5 promotes the growth of colorectal cancer cells by inhibiting the generation of spermidine in TAMS [30]. In breast cancer, the expression of ODC that regulates the synthetic polyamine metabolism is significantly higher than in non-tumor tissues. The activity of PAOX and SMOX that regulate the polyamine decomposition is reduced, which is positively related to the tumor invasion [31]. The results of this study reveal the change of PMRG in the transcription level in HCC. Compared to normal tissues, we also found that genes involved in polyamine synthesis were up-regulated, and genes involved in polyamine catabolism and transport were downregulated. We identified three different molecular subtypes based on 35 genes associated with polyamine metabolism and found that cluster1 was associated with high levels of PMRG expression and higher tumor grading and TNM staging. TME characteristics also differed significantly between different subtypes. In addition, cluster1 is significantly enriched with immune total activation-related molecular signaling pathways. At the same time, some immune-related biological processes are significantly enriched in cluster1. These results also support the liver as an immune organ with a wealth of innate immune cells, and hepatocellular carcinoma coordinates the innate and acquired immune response [32].

The difference analysis of this study showed that the expression of NNMT, CXCL1, CXCL8, CCL20, and CD24 in cluster1 increased significantly. It has been reported that the synthesis of polyamines can be regulated by regulating the expression of nicotinamide N-methyltransferase (NNMT) [33]. The expression of NNMT in various cancers such as ovarian, colon, liver, stomach, and thyroid cancers has been associated with poor prognosis [34, 35]. DNA methylation mediated by NNMT regulates the expression of pro-tumor cytokines, resulting in a significant reduction in tumor suppressor protein phosphatase 2A (PP2A) activity [36, 37]. Stromal NNMT expression promotes the expression of cancer-associated fibroblast (CAF) markers and the secretion of cytokines and the extracellular matrix of cancer causative cells, thereby promoting the growth and metastasis of ovarian cancer [38]. In liver and colon cancers, NNMT expression is associated with the initiation of signal transducer and activator of transcription 3 (STAT3) [39]. Elevated chemokines CXCL1 and CXCL8 promote the transfer of HCC and poor prognosis [40, 41]. CCL20 is an HCV-induced pro-angiogenesis chemokine that promotes the onset and development of HCC by recruiting CCR6 B lymphocytes to the microenvironment [42]. CD24 expression levels were positively correlated with sorafenib resistance, and CD24 overexpression modulated sorafenib resistance by upregulating PPA protein levels and inducing inactivation of the mTOR/AKT pathway to activate autophagy in hepatocellular carcinoma [43]. Significantly upregulated NNMT, CXCL1, CXCL8, CCL20, and CD24 in cluster1 may be associated with their poor survival, and as such, they may become prognostic biomarkers for potential HCC.

The interaction between cancer cells and host immune responses can inhibit cancer progression in the tumor microenvironment. In recent years, immune checkpoints have been reported to inhibit anti-tumor immune responses in solid tumors, such as PD-1 and PD-L1. The CTLA-4 pathway is primarily involved in T cell-mediated regulation of the immune response, and the PD-1 pathway is involved mainly in inhibiting T cell activation in peripheral tissues [44]. PD-1 blocks the "cancer immune cycle" by inhibiting the migration of T cells by binding to PD-L1 [45].In the tumor microenvironment of HCC, PD-1 and PD-L1 are highly expressed in CD8+ T cells, Kupffer cells, and inflammatory cells within tumors, resulting in impaired effector T cell function in HCC and invasion of tumor cells [46]. CTLA-4 binds to CD80/CD86 on dendritic cells, inhibiting T cells and controlling excessive immune responses. Downregulation of other immune checkpoints such as TIGIT expression can prevent dysfunction of HCC-induced CD8+ T cells and natural killer cells [47], and ICOS is upregulated in Tregs-infiltrated HCC [48]. These immune checkpoints are likely to serve as potential targets for anti-tumor therapies. We also compared immune infiltration between low-risk groups and high-risk groups. Compared to low-risk patients, the proportion of memory B cells, CD4+ memory activated T cells, follicular helper T cells, monocytes, M0 macrophages, resting dendritic cells, and neutrophils in high-risk HCC patients was generally higher ($p<0.05$). In contrast, the proportion of naive B cells, CD8+T cells, resting mast cells, activated NK cells and M1 macrophages were lower than that in low-risk patients ($p<0.05$). Previous studies have shown that CD4 memory resting T cells can further differentiate and perform various functions, including blocking the activation of CD8+ T cells and NK cell killing, helping CD8+ T cells participate in tumor rejection, and inhibiting harmful immune responses to autoantigens and external antigens [49, 50]. The above results indicate that the PMRG score is consistent with immune checkpoints expression capacity and immune cell infiltration. It seems to indicate that the poor prognosis may be result from the higher expression of immune checkpoints

and its immunosuppressive microenvironment. Therefore, compared with low-risk patients, high-risk patients may have better prognosis from immune checkpoint inhibitor treatment.

7. Conclusion

The PMRGs may play an immunosuppressive role in HCC, and patients with high PMRGs expression are more likely to benefit from immune checkpoint inhibitors. Our study reflects the intensity of the immune response triggered by gene states related to polyamine metabolism in the hepatocellular carcinoma microenvironment, providing new insights for understanding the immune microenvironment of liver cancer and immune-related therapy and providing new indicators for judging the prognosis of patients.

8. Funding Statement

This work was supported by the Shandong Key Research and Development Program (2019GSF108218, 2019GSF108139), Taishan Scholar Program of Shandong Province, Natural Science Foundation of Shandong Province (ZR2020MH007), and Natural Science Foundation of China (Grant No. 81874040, 82172350).

References

1. Sung H, Ferlay J, Siegel RL, Laversanne M, Soerjomataram I, Jemal A, et al. Global Cancer Statistics 2020: GLOBOCAN Estimates of Incidence and Mortality Worldwide for 36 Cancers in 185 Countries. CA Cancer J Clin. 2021; 71(3): 209-49.
2. El-Serag HB, Rudolph KL. Hepatocellular carcinoma: epidemiology and molecular carcinogenesis. Gastroenterology. 2007; 132(7): 2557-76.
3. Park EJ, Lee JH, Yu GY, He G, Ali SR, Holzer RG, et al. Dietary and genetic obesity promote liver inflammation and tumorigenesis by enhancing IL-6 and TNF expression. Cell. 2010; 140(2): 197-208.
4. Degasperi E, Colombo M. Distinctive features of hepatocellular carcinoma in non-alcoholic fatty liver disease. Lancet Gastroenterol Hepatol. 2016; 1(2): 156-64.
5. Khemlina G, Ikeda S, Kurzrock R. The biology of Hepatocellular carcinoma: implications for genomic and immune therapies. Mol Cancer. 2017; 16(1): 149.
6. Tang W, Chen Z, Zhang W, Cheng Y, Zhang B, Wu F, et al. The mechanisms of sorafenib resistance in hepatocellular carcinoma: theoretical basis and therapeutic aspects. Signal Transduct Target Ther. 2020; 5(1): 87.
7. Llovet JM, Ricci S, Mazzaferro V, Hilgard P, Gane E, Blanc JF, et al. Sorafenib in advanced hepatocellular carcinoma. N Engl J Med. 2008; 359(4): 378-90.
8. Nakamura K, Smyth MJ. Myeloid immunosuppression and immune checkpoints in the tumor microenvironment. Cell Mol Immunol. 2020; 17(1): 1-12.
9. Zhou SL, Zhou ZJ, Hu ZQ, Huang XW, Wang Z, Chen EB, et al. Tumor-Associated Neutrophils Recruit Macrophages and T-Regulatory Cells to Promote Progression of Hepatocellular Carcinoma and Resistance to Sorafenib. Gastroenterology. 2016; 150(7): 1646-58 e17.
10. Chen Y, Ramjiawan RR, Reiberger T, Ng MR, Hato T, Huang Y, et al. CXCR4 inhibition in tumor microenvironment facilitates anti-programmed death receptor-1 immunotherapy in sorafenib-treated hepatocellular carcinoma in mice. Hepatology. 2015; 61(5): 1591-602.
11. Dong N, Shi X, Wang S, Gao Y, Kuang Z, Xie Q, et al. M2 macrophages mediate sorafenib resistance by secreting HGF in a feed-forward manner in hepatocellular carcinoma. Br J Cancer. 2019; 121(1): 22-33.
12. Hato T, Goyal L, Greten TF, Duda DG, Zhu AX. Immune checkpoint blockade in hepatocellular carcinoma: current progress and future directions. Hepatology. 2014; 60(5): 1776-82.
13. Hodi FS, O'Day SJ, McDermott DF, Weber RW, Sosman JA, Haanen JB, et al. Improved survival with ipilimumab in patients with metastatic melanoma. N Engl J Med. 2010; 363(8): 711-23.
14. Motzer RJ, Escudier B, McDermott DF, George S, Hammers HJ, Srinivas S, et al. Nivolumab versus Everolimus in Advanced Renal-Cell Carcinoma. N Engl J Med. 2015; 373(19): 1803-13.
15. Brahmer J, Reckamp KL, Baas P, Crino L, Eberhardt WE, Poddubskaya E, et al. Nivolumab versus Docetaxel in Advanced Squamous-Cell Non-Small-Cell Lung Cancer. N Engl J Med. 2015; 373(2): 123-35.
16. Huang MY, Jiang XM, Wang BL, Sun Y, Lu JJ. Combination therapy with PD-1/PD-L1 blockade in non-small cell lung cancer: strategies and mechanisms. Pharmacol Ther. 2021; 219: 107694.
17. Carlino MS, Larkin J, Long GV. Immune checkpoint inhibitors in melanoma. Lancet. 2021; 398(10304): 1002-14.
18. Pegg AE, Casero RA, Jr. Current status of the polyamine research field. Methods Mol Biol. 2011; 720: 3-35.
19. Novita Sari I, Setiawan T, Seock Kim K, Toni Wijaya Y, Won Cho K, Young Kwon H. Metabolism and function of polyamines in cancer progression. Cancer Lett. 2021; 519: 91-104.
20. Sandsmark E, Hansen AF, Selnaes KM, Bertilsson H, Bofin AM, Wright AJ, et al. A novel non-canonical Wnt signature for prostate cancer aggressiveness. Oncotarget. 2017; 8(6): 9572-86.
21. Zabala-Letona A, Arruabarrena-Aristorena A, Martin-Martin N, Fernandez-Ruiz S, Sutherland JD, Clasquin M, et al. mTORC1-dependent AMD1 regulation sustains polyamine metabolism in prostate cancer. Nature. 2017; 547(7661): 109-13.
22. Zabala-Letona A, Arruabarrena-Aristorena A, Martin-Martin N, Fernandez-Ruiz S, Sutherland JD, Clasquin M, et al. Corrigendum: mTORC1-dependent AMD1 regulation sustains polyamine metabolism in prostate cancer. Nature. 2018; 554(7693): 554.
23. Casero RA, Jr., Murray Stewart T, Pegg AE. Polyamine metabolism and cancer: treatments, challenges and opportunities. Nat Rev Cancer. 2018; 18(11): 681-95.
24. Soda K. The mechanisms by which polyamines accelerate tumor spread. J Exp Clin Cancer Res. 2011; 30: 95.
25. Zhou S, Gu J, Liu R, Wei S, Wang Q, Shen H, et al. Spermine Alleviates Acute Liver Injury by Inhibiting Liver-Resident Macrophage Pro-Inflammatory Response Through ATG5-Dependent Autophagy. Front Immunol. 2018; 9: 948.

26. Chia TY, Zolp A, Miska J. Polyamine Immunometabolism: Central Regulators of Inflammation, Cancer and Autoimmunity. Cells. 2022; 11(5).
27. Murray-Stewart T, Dunworth M, Lui Y, Giardiello FM, Woster PM, Casero RA, Jr. Curcumin mediates polyamine metabolism and sensitizes gastrointestinal cancer cells to antitumor polyamine-targeted therapies. PLoS One. 2018; 13(8): e0202677.
28. Bruix J, Sherman M, American Association for the Study of Liver D. Management of hepatocellular carcinoma: an update. Hepatology. 2011; 53(3): 1020-2.
29. Long J, Lin J, Wang A, Wu L, Zheng Y, Yang X, et al. PD-1/PD-L blockade in gastrointestinal cancers: lessons learned and the road toward precision immunotherapy. J Hematol Oncol. 2017; 10(1): 146.
30. Miao H, Ou J, Peng Y, Zhang X, Chen Y, Hao L, et al. Macrophage ABHD5 promotes colorectal cancer growth by suppressing spermidine production by SRM. Nat Commun. 2016; 7: 11716.
31. Cervelli M, Pietropaoli S, Signore F, Amendola R, Mariottini P. Polyamines metabolism and breast cancer: state of the art and perspectives. Breast Cancer Res Treat. 2014; 148(2): 233-48.
32. Inada Y, Mizukoshi E, Seike T, Tamai T, Iida N, Kitahara M, et al. Characteristics of Immune Response to Tumor-Associated Antigens and Immune Cell Profile in Patients With Hepatocellular Carcinoma. Hepatology. 2019; 69(2): 653-65.
33. Kraus D, Yang Q, Kong D, Banks AS, Zhang L, Rodgers JT, et al. Nicotinamide N-methyltransferase knockdown protects against diet-induced obesity. Nature. 2014; 508(7495): 258-62.
34. Roberti A, Fernandez AF, Fraga MF. Nicotinamide N-methyltransferase: At the crossroads between cellular metabolism and epigenetic regulation. Mol Metab. 2021; 45: 101165.
35. Kim J, Hong SJ, Lim EK, Yu YS, Kim SW, Roh JH, et al. Expression of nicotinamide N-methyltransferase in hepatocellular carcinoma is associated with poor prognosis. J Exp Clin Cancer Res. 2009; 28: 20.
36. Palanichamy K, Kanji S, Gordon N, Thirumoorthy K, Jacob JR, Litzenberg KT, et al. NNMT Silencing Activates Tumor Suppressor PP2A, Inactivates Oncogenic STKs, and Inhibits Tumor Forming Ability. Clin Cancer Res. 2017; 23(9): 2325-34.
37. Ulanovskaya OA, Zuhl AM, Cravatt BF. NNMT promotes epigenetic remodeling in cancer by creating a metabolic methylation sink. Nat Chem Biol. 2013; 9(5): 300-6.
38. Eckert MA, Coscia F, Chryplewicz A, Chang JW, Hernandez KM, Pan S, et al. Proteomics reveals NNMT as a master metabolic regulator of cancer-associated fibroblasts. Nature. 2019; 569(7758): 723-8.
39. Tomida M, Ohtake H, Yokota T, Kobayashi Y, Kurosumi M. Stat3 up-regulates expression of nicotinamide N-methyltransferase in human cancer cells. J Cancer Res Clin Oncol. 2008; 134(5): 551-9.
40. He Q, Huang W, Liu D, Zhang T, Wang Y, Ji X, et al. Homeobox B5 promotes metastasis and poor prognosis in Hepatocellular Carcinoma, via FGFR4 and CXCL1 upregulation. Theranostics. 2021; 11(12): 5759-77.
41. Li XP, Yang XY, Biskup E, Zhou J, Li HL, Wu YF, et al. Co-expression of CXCL8 and HIF-1alpha is associated with metastasis and poor prognosis in hepatocellular carcinoma. Oncotarget. 2015; 6(26): 22880-9.
42. He H, Wu J, Zang M, Wang W, Chang X, Chen X, et al. CCR6(+) B lymphocytes responding to tumor cell-derived CCL20 support hepatocellular carcinoma progression via enhancing angiogenesis. Am J Cancer Res. 2017; 7(5): 1151-63.
43. Lu S, Yao Y, Xu G, Zhou C, Zhang Y, Sun J, et al. CD24 regulates sorafenib resistance via activating autophagy in hepatocellular carcinoma. Cell Death Dis. 2018; 9(6): 646.
44. Buchbinder EI, Desai A. CTLA-4 and PD-1 Pathways: Similarities, Differences, and Implications of Their Inhibition. Am J Clin Oncol. 2016; 39(1): 98-106.
45. Butte MJ, Keir ME, Phamduy TB, Sharpe AH, Freeman GJ. Programmed death-1 ligand 1 interacts specifically with the B7-1 costimulatory molecule to inhibit T cell responses. Immunity. 2007; 27(1): 111-22.
46. Wu K, Kryczek I, Chen L, Zou W, Welling TH. Kupffer cell suppression of CD8+ T cells in human hepatocellular carcinoma is mediated by B7-H1/programmed death-1 interactions. Cancer Res. 2009; 69(20): 8067-75.
47. Han Q, Wang Y, Pang M, Zhang J. STAT3-blocked whole-cell hepatoma vaccine induces cellular and humoral immune response against HCC. J Exp Clin Cancer Res. 2017; 36(1): 156.
48. Pedroza-Gonzalez A, Kwekkeboom J, Sprengers D. T-cell suppression mediated by regulatory T cells infiltrating hepatic tumors can be overcome by GITRL treatment. Oncoimmunology. 2013; 2(1): e22450.
49. Crouse J, Xu HC, Lang PA, Oxenius A. NK cells regulating T cell responses: mechanisms and outcome. Trends Immunol. 2015; 36(1): 49-58.
50. Rosenberg J, Huang J. CD8(+) T Cells and NK Cells: Parallel and Complementary Soldiers of Immunotherapy. Curr Opin Chem Eng. 2018; 19: 9-20.